



Synthesis, characterization, DNA binding and antitumor activities of Cu(II) complexes

A.F. Shoair^{a,b,*}, A.A. El-Bindary^a, N.A. El-Ghamaz^c, G.N. Rezk^a

^a Chemistry Department, Faculty of Science, Damietta University, Damietta 34517, Egypt

^b Chemistry Department, Faculty of Science, Taif University, Saudi Arabia

^c Physics Department, Faculty of Science, Damietta University, Damietta 34517, Egypt

ARTICLE INFO

Article history:

Received 16 May 2018

Received in revised form 6 July 2018

Accepted 11 August 2018

Available online 17 August 2018

Keywords:

Cu(II) complexes
Molecular structure
DNA binding
Antitumor activities

ABSTRACT

A series of Cu(II) complexes of 5,5-dimethyl-2-(2-arylhydrazono)cyclohexane-1,3-dione (HL_n) were synthesized by the coupling of dimedone with aniline and its derivatives. These ligands and their Cu(II) complexes were characterized by elemental analyses, IR, ¹H NMR, ¹³C NMR, UV-Visible, X-ray diffraction analysis and magnetic measurements. Spectral studies revealed that the ligand exist in an internally hydrogen bonded keto-hydrazone form rather than the azo-enol form. The ligands (HL_n) acts as a monobasic bidentate ligand by coordinating via the nitrogen atom of the hydrazone moiety (—NH—) with deprotonation and oxygen atom of the carbonyl (C=O) group. The optimized bond lengths, bond angles and quantum chemical parameters of the complexes were calculated. The calf thymus DNA binding activity of the ligands and their Cu(II) complexes were studied by absorption spectra and viscosity measurements. The antimicrobial activities of ligands and Cu(II) complexes were tested against Gram negative bacteria (*Escherichia coli*), Gram positive bacteria (*Staphylococcus aureus*) and fungal (*Candida albicans*). The cytotoxic activity of ligands and Cu(II) complexes was tested against two human cancer HePG-2 (Hepatocellular carcinoma) and MCF-7 (breast cancer). The antioxidant activities of ligands and Cu(II) complexes were performed by ABTS method.

© 2018 Elsevier B.V. All rights reserved.

1. Introduction

β -Diketones are interesting compounds in view of their chemical stability, facile preparation [1] and their possible functionalization in the three different sites of the molecule [2]. By far, the most widely known is the dimedone that exhibits interesting and specific properties, such as pharmacological activities like antibacterial, antiviral, antioxidant and antitumor activities [3]. One of the most important features of 1,3-diketones is the keto-enol tautomerism [4]. The diketo/ketoenol equilibrium is in general strongly shifted towards the enol form due to resonance-assisted hydrogen bonding, facilitating the formation of a pseudo six-membered ring [5]. The equilibrium can, however, be affected by other factors where the most important are the solvent polarity and the nature of substituents (both terminal and central ones) [6]. Meanwhile, the close values of M—O bond lengths in chelating rings of β -diketone complexes usually prevent the estimate of the contribution of a certain tautomeric form.

Arylhydrazones of methylene active compounds are compounds of great potential in organic chemistry [7] and with many possible

applications, e.g. related to tautomerism and isomerism [8], strong intramolecular N—H...O resonance assisted hydrogen bonding [9]. Thus, they can be used as ionophores for ion-selective electrodes and micro-electrodes, solvatochromic agents, analytical reagents [10]. Arylhydrazones of methylene active compounds can also be applied as valuable ligands due to their reach coordination ability and generally higher stability than that of the related β -diketones [10]. Many complexes of arylhydrazones of methylene active compound possess interesting structural, magnetic and/or catalytic properties. For instance, they behave as active catalysts of the Henry reaction or in the oxidation of alkanes and alcohols [11].

Chemistry of Cu(II) complexes is of significant importance, because of the fascinating reactivity exhibited by the resultant complexes and the nature of the ligands that dictates the property of those complexes [12]. The Copper complexes have applications in the fields of biochemistry, photochemistry and photophysics [13]. The last few decades have seen an increased interest in copper(II) acetate complexes as building blocks in supramolecular devices due to their favorable excited state and redox properties as well as structural probes for DNA. Copper complexes are also showing promising results in anti-tumor activity and they target a broad spectrum of cancers [14].

Herein, we report the synthesis and characterization of 5,5-dimethyl-2-(2-arylhydrazono)cyclohexane-1,3-dione (HL_n) and their Cu

* Corresponding author at: Chemistry Department, Faculty of Science, Damietta University, Damietta 34517, Egypt.

E-mail address: abdel_shoair@yahoo.com (A.F. Shoair).

(II) complexes by different spectroscopic techniques. The optimized bond lengths, bond angles and quantum chemical parameters of the complexes were calculated. The calf thymus DNA binding activities were studied. The thermodynamic parameters of the ligands (\mathbf{HL}_n) and their Cu(II) complexes are calculated using Coats–Redfern and Horowitz-Metzger methods. Molecular docking was used to predict the binding between arylhydrazone compounds (\mathbf{HL}_n) with the receptor of 3qum-IMMUNE SYSTEM and human prostate specific antigen (PSA). The antimicrobial activities of ligands were tested against Gram negative bacteria (*Escherichia coli*), Gram positive bacteria (*Staphylococcus aureus*) and fungal (*Candida albicans*).

2. Experimental

2.1. Materials and apparatus

All reagents were purchased from Aldrich, Fluka and Merck and were used without any further purification. Micro analytical data (C, H and N) were collected on Automatic Analyzer CHNS Vario ELIII, Germany. The amount of copper for each stoichiometric determination was determined using Flame Atomic Absorption spectrophotometer (Model Varian AA240FS). Spectroscopic data were obtained using the following instruments: FTIR spectra (KBr discs, 4000–400 cm^{-1}) by Jasco FTIR-4100 spectrophotometer; the ^1H NMR and ^{13}C NMR spectra by Bruker WP operating at 300 and 75 MHz, respectively using DMSO- d_6 as a solvent. The chemical shifts are reported in ppm using tetramethylsilane (TMS) as the internal reference; UV-Visible spectra by Perkin-Elmer AA800 spectrophotometer Model AAS, using a 1.0 cm cell. Structural variations of the as-prepared materials were examined using X-ray diffraction (XRD) technique. The XRD patterns of the powder were recorded on Siemens X-ray diffractometer D-500 equipped with Cu K_α radiation source. The crystal system, space group and lattice parameters values of the complexes were calculated and optimized using CRYSFIRE and CHEKCELL computer programs [15]. The molecular structures of the investigated Cu(II) complexes were optimized by HF method with 3-21G basis set. The molecules were built with the Perkin Elmer ChemBio Draw and optimized using Perkin Elmer ChemBio3D software [16]. Thermal analysis of the ligands and their Cu(II) complexes were carried out using a Shimadzu thermogravimetric analyzer under a nitrogen atmosphere with heating rate of 10 $^\circ\text{C}/\text{min}$ over a temperature range from room temperature up to 800 $^\circ\text{C}$. Magnetic susceptibility measurements were determined at room temperature on a Johnson Matthey magnetic susceptibility balance using $\text{Hg}[\text{Co}(\text{SCN})_4]$ as calibrant. Effective magnetic moments were calculated based on the equation: $\mu_{\text{eff}} = 2.84 (X_M^{\text{corr}} T)^{1/2}$. Conductivity measurements of the complexes at 25 ± 1 $^\circ\text{C}$ were determined in DMF (10^{-3} M) using conductivity/TDS meter model Lutron YK-22CT. The pH values were measured with a pH meter (Jenway Model: 3020) supplied with a glass-combined electrode. Docking simulation was performed using MGL tools 1.5.4 with AUTOGRIID 4 and AUTODOCK version 4.2. The DNA sequence obtained from the Protein Data Bank (PDB NDB: DD0018) and the ligands were optimized by SPARTAN 10 program and both the ligands and DNA were prepared for using in AUTODOCK tools. The DNA was enclosed in a box with number of grid points in $x \times y \times z$ directions, $20 \times 20 \times 20$.

2.2. Preparation of the arylhydrazone derivatives (\mathbf{HL}_n)

The ligands (\mathbf{HL}_n) were synthesized according to the Japp-Klingemann reaction [17,18] between the diazonium salt of aniline derivatives and 5,5-dimethylcyclohexane-1,3-dione (dimedone). Dimedone (1.40 g, 0.01 mol) was dissolved in 50 mL ethanol solution of NaOH (0.4 g, 0.01 mol) and sodium acetate (3.65 g, 0.01 mol). The resulting β -diketonate solution was diluted with water to a volume of about 150 mL and cooled to 0 $^\circ\text{C}$. The diazonium salt solution was prepared separately by addition of a saturated aqueous solution of sodium nitrite (0.69 g, 0.01 mol) to a cooled solution (0 $^\circ\text{C}$) of the desired aniline

derivatives (0.01 mol) in 10 mL hydrochloric acid (5 M). The solution of the diazonium salt was then added dropwise to the β -diketonate solution with vigorous stirring for 1 h. The colored precipitate, which was formed immediately, was filtered through sintered glass gooch, washed several times with water and ethanol then dried in a vacuum desiccator over anhydrous CaCl_2 . The products were purified by recrystallization from ethanol (Fig. 1).

The resulting formed ligands are:

$\mathbf{HL}_1 = 5,5\text{-dimethyl-2-(2-(4-methylphenyl)hydrazono)cyclohexane-1,3-dione}$.

$\mathbf{HL}_2 = 5,5\text{-dimethyl-2-(2-phenylhydrazono)cyclohexane-1,3-dione}$.

$\mathbf{HL}_3 = 5,5\text{-dimethyl-2-(2-(4-chlorophenyl)hydrazono)-cyclohexane-1,3-dione}$.

2.3. Preparation of Cu(II) complexes (1–3)

Copper(II) complexes (Fig. 2) were synthesized according to the general procedure [18,19]. A stoichiometric amount of the desired ligand (0.01 mol) in ethanol (20 cm^3) was added dropwise to a hot ethanol solution (20 cm^3) of $\text{Cu}(\text{OAc})_2 \cdot 2\text{H}_2\text{O}$ (0.01 mol) with stirring and the reaction mixture was refluxed for 3 h. The solution was concentrated to half of its original volume by evaporation and kept in air at room temperature for slow evaporation for 2 days. During this, a microcrystalline solid was separated, which was isolated by filtration, washed with ethanol, ether and dried in a vacuum desiccator over anhydrous CaCl_2 .



2.4. DNA binding experiments

The binding properties of the ligands and their Cu(II) complexes to CT-DNA have been studied using electronic absorption spectroscopy. The stock solution of CT-DNA was prepared in 5 mM Tris-HCl/50 mM NaCl buffer (pH = 7.2), which a ratio of UV absorbance at 260 and 280 nm (A_{260}/A_{280}) of ca. 1.8–1.9, indicating that the DNA was sufficiently free of protein [20], and the concentration was determined by UV absorbance at 260 nm ($\epsilon = 6600 \text{ M}^{-1} \cdot \text{cm}^{-1}$) [21]. Electronic absorption spectra (200–700 nm) were carried out using 1 cm quartz cuvettes at 25 $^\circ\text{C}$ by fixing the concentration of ligand or complex, while gradually increasing the concentration of CT-DNA. An equal amount of CT-DNA was added to both the compound solutions and the references buffer solution to eliminate the absorbance of CT-DNA itself. For every addition, the mixture was shaken and allowed to keep for 10 min at room temperature, and then the absorption spectra were recorded. The intrinsic binding constant K_b of the compounds with CT-DNA was determined using the following Eq. (1) [22]:

$$[\text{DNA}]/(\epsilon_a - \epsilon_f) = [\text{DNA}]/(\epsilon_b - \epsilon_f) + 1/K_b(\epsilon_a - \epsilon_f) \quad (1)$$

where [DNA] is the concentration of CT-DNA in base pairs, ϵ_a is the extinction coefficient observed for the $A_{\text{obs}} / [\text{compound}]$ at the given DNA concentration, ϵ_f is the extinction coefficient of the free compound in solution and ϵ_b is the extinction coefficient of the compound when fully bond to DNA. In plots of $[\text{DNA}] / (\epsilon_a - \epsilon_f)$ vs. [DNA], K_b is given by the ratio of the slope to the intercept.

2.5. Viscosity measurements

Viscosity measurements were performed at compound concentration within the range of $(0.1\text{--}0.6 \times 10^{-4} \text{ mol/L})$ and each compound was added into a DNA solution (10^{-3} mol/L) present in the viscometer. The average flow times of three replicates were measured with a digital stopwatch. The data were presented as $(\eta/\eta_0)^{1/3}$ vs. $[\text{compound}]/[\text{DNA}]$

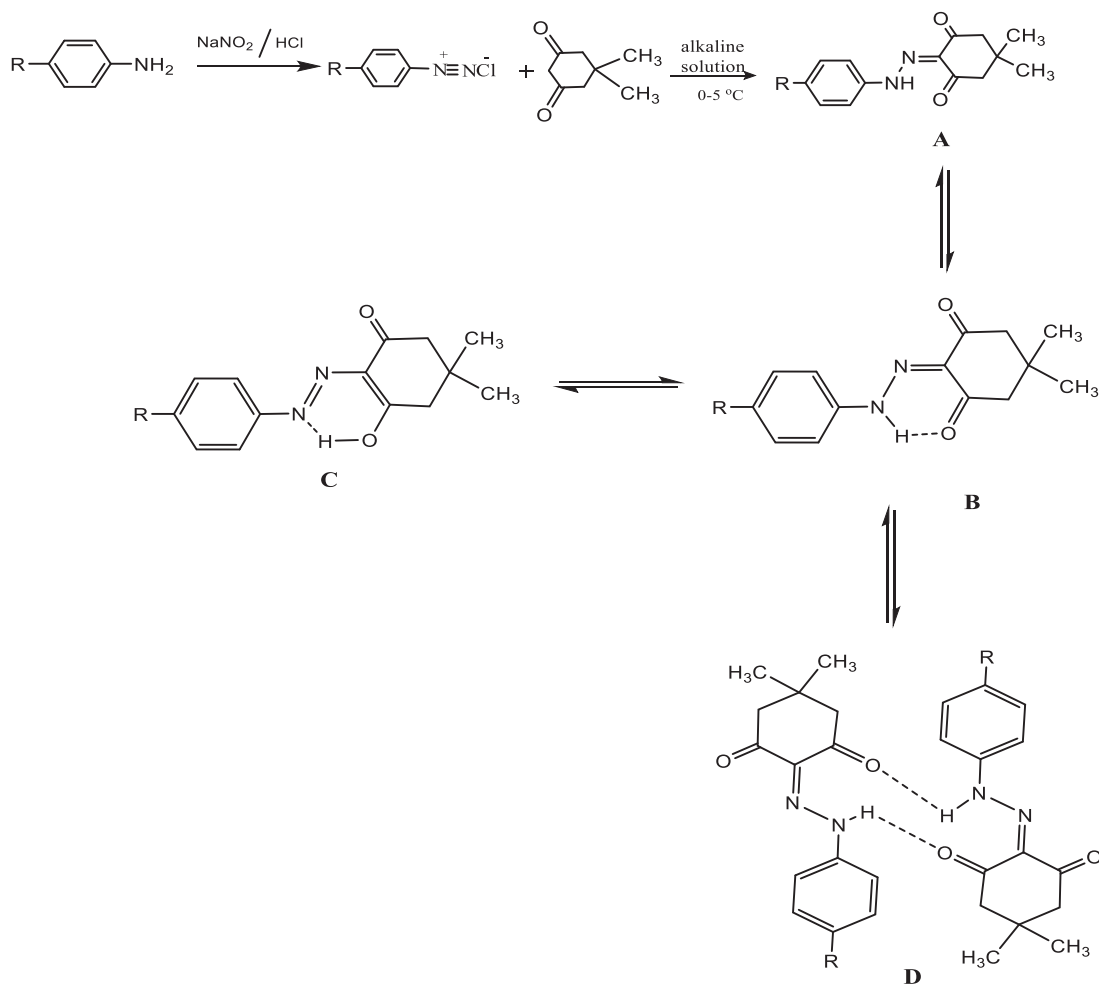


Fig. 1. The formation mechanism of the ligands (**HL**_n).

ratio of the concentration of the compound to DNA [23], where η and η_0 are the viscosity of the DNA in the presence and absence of complex, respectively [24]. The relative viscosities η were calculated using equation [25]:

$$\eta = (t - t_0) / t_0 \quad (2)$$

where t is the observed flow time of DNA containing solution and t_0 is the flow time of buffer alone.

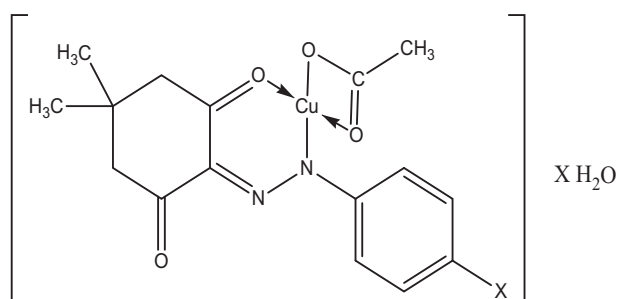


Fig. 2. The proposed structure of the complexes $[\text{Cu}(\text{L}_n)(\text{CH}_3\text{COO})]\text{X}\cdot\text{H}_2\text{O}$ (1–3).

2.6. Antimicrobial investigation

The ligands and their Cu(II) complexes were individually tested against Gram negative rod (*Escherichia coli*) bacteria, Gram positive cocci (*Staphylococcus aureus*) and yeast (*Candida albicans*). Each of the compounds was dissolved in DMSO (1 mg/mL) and paper discs of Whatman filter paper were prepared with standard size (5 cm) and sterilized in an autoclave. The paper discs were soaked and placed aseptically in the petri dishes containing nutrient and Dox's agar media (agar 20 g, beef extract 3 g and peptone 5 g) seeded with *Staphylococcus aureus*, *E. coli* and *Candida albicans*. The petri dishes were incubated at $36 \pm 1^\circ\text{C}$ and the inhibition zones were recorded after 24 h of incubation. Each treatment was replicated three times. The antibacterial activity of a common standard antibiotic ampicillin and antifungal clotrimazole was also recorded using the same procedure. The % activity index for the compound was calculated using the following Eq. (3):

$$\% \text{Activity Index} = \frac{\text{Zone of inhibition by test compound (diameter)}}{\text{Zone of inhibition by standard (diameter)}} \times 100 \quad (3)$$

Table 1
Physical properties and elemental analyses data of the ligands (HL_n) and their Cu(II) complexes (1–3).

Comp.	Structure	Molecular formula	Mol. weight	M.P. (°C)	Yield (%)	Color	Exp. (Calcd.) (%)				$\Lambda_M \Omega^{-1} \text{cm}^2 \text{mol}^{-1}$	μ_{eff} B.M.
							C	H	N	Cu		
HL ₁	5,5 Dimethyl 2 (2 (p tolyl)hydrazono) cyclohexane 1,3 dione	C ₁₅ H ₁₈ N ₂ O ₂	258.32	158	70	Orange	(69.75) 69.88	(7.02) 6.97	(10.84) 10.82	–	–	–
HL ₂	5,5 Dimethyl 2 (2 phenylhydrazono) cyclohexane 1,3 dione	C ₁₄ H ₁₆ N ₂ O ₂	244.29	146	65	Brown	(68.83) 69.17	(6.60) 6.51	(11.46) 11.75	–	–	–
HL ₃	2 (2 (4 Chlorophenyl) hydrazono) 5,5 dimethylcyclohexane 1,3 dione	C ₁₄ H ₁₅ ClN ₂ O ₂	278.74	228	67	Yellow	(60.33) 60.66	(5.42) 5.35	(10.05) 10.04	–	–	–
(1)	[Cu(L ₁)(CH ₃ COO)] 2H ₂ O	C ₁₇ H ₂₄ CuN ₂ O ₆	415.93	>300	72	Brown	(49.09) 48.84	(5.81) 5.34	(6.73) 5.92	(15.28) 15.30	12	1.70
(2)	[Cu(L ₂)(CH ₃ COO)]	C ₁₆ H ₁₈ CuN ₂ O ₄	365.87	>300	70	Green	(52.53) 52.15	(4.96) 4.99	(7.65) 7.52	(17.37) 17.34	16	1.72
(3)	[Cu(L ₃)(CH ₃ COO)] H ₂ O	C ₁₆ H ₁₉ ClCuN ₂ O ₅	418.33	>300	78	Brown	(45.94) 46.30	(4.58) 4.42	(6.70) 6.52	(15.19) 15.22	12	1.78

2.7. Cytotoxicity investigation

2.7.1. Cell lines and chemical reagents

Mammalian cell lines: HepG-2 cells (human Hepatocellular carcinoma) and MCF-7 cells (human Breast carcinoma) were obtained from ATCC via Holding company for biological products and vaccines (VACSERA), Cairo, Egypt. Chemical reagents; RPMI-1640 medium, MTT, DMSO and 5-fluorouracil were purchased from Sigma chemicals (St. Louis, USA), Fetal Bovine serum (FBS) was purchased from (GIBCO, UK). 5-Fluorouracil (5-FU) was used as a standard anticancer drug for comparison. All the compounds and the standard dissolved in DMSO, diluted with culture medium containing 0.1% DMSO. The control cells were treated with culture medium containing 0.1% DMSO.

2.7.2. MTT assay

The cell lines mentioned above were used to determine the inhibitory effects of ligands and their Cu(II) complexes on cell growth using the MTT assay [26]. The following colorimetric assay is based on the conversion of the yellow tetrazolium bromide to a purple formazan derivative by mitochondrial succinate dehydrogenase in viable cells. Cell lines were cultured in RPMI-1640 medium with 10% fetal bovine serum. Antibiotics added were 100 units/mL penicillin and 100 µg/mL streptomycin at 37 °C in a 5% CO₂ incubator. The cell lines were seeded in a 96-well plate at a density of 1.0×10^4 cells/well at 37 °C for 48 h under 5% CO₂, followed by 24 h incubation with the indicated drug doses [27]. At the end of the drug treatment, 20 µL of MTT solution at

5 mg/mL was added and incubated for 4 h. Dimethyl sulfoxide (DMSO) in volume of 100 µL is added into each well to dissolve the purple formazan formed. The colorimetric assay is measured and recorded as absorbance at 570 nm using a plate reader (EXL 800). Cytotoxicity was expressed as IC₅₀ (µg/mL) which indicates the concentration of the compound that inhibited proliferation rate of the tumor cells by 50% as compared to the control untreated cells. IC₅₀ values were determined from the plot: % relative cell viability (% inhibition concentration) vs. compound concentration. The relative cell viability values were calculated using Eq. (4):

$$\% \text{The relative cell viability} = \frac{A(570 \text{ nm}) \text{ of treated samples}}{A(570 \text{ nm}) \text{ of untreated sample}} \times 100 \quad (4)$$

2.8. Anti-oxidant activity screening assay - ABTS method

Antioxidant activity screening assay ABTS method [28] was used for determination of scavenging activity of ligands and their Cu(II) complexes. For each of the investigated compounds (2 mL) of ABTS (2,2'-azinobis-(3-ethyl-benzothiazoline-6-sulphonic acid) solution (60 µM) was added to 3 mL MnO₂ solution (25 mg/mL), all prepared in (5 mL) aqueous phosphate buffer solution (pH 7, 0.1 M). The mixture was

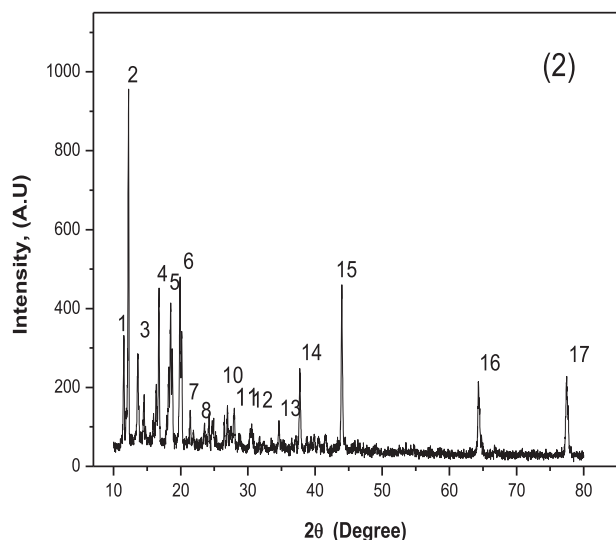


Fig. 3. X-ray diffraction patterns of complex (2).

Table 2
Crystallographic data for complex (2).

System: monoclinic		Space group: <i>p</i> 21	
a = 14.6315 Å b = 7.0358 Å		α = 90° β = 100.53° γ = 90°	
c = 8.1280 Å			
Peak no.	2θ (°)	d (Å)	(hkl)
1	11.5247	7.6721	$\bar{1}$ 0 1
2	12.2072	7.2447	2 0 0
3	13.6149	6.4986	1 0 1
4	16.7417	5.2913	0 1 1
5	18.4988	4.7925	3 0 0
6	19.9231	4.4529	$\bar{3}$ 0 1
7	23.5248	3.7787	$\bar{3}$ 1 1
8	24.1980	3.6751	1 0 2
9	24.7498	3.5944	4 0 0
10	26.4858	3.3626	3 1 1
11	27.9359	3.1912	$\bar{1}$ 2 1
12	30.4964	2.9289	2 1 2
13	34.6192	2.5889	3 2 1
14	37.7435	2.3815	$\bar{3}$ 1 3
15	43.9876	2.1715	$\bar{3}$ 2 3
16	64.3597	2.0568	$\bar{8}$ 1 4
17	77.4734	1.4464	$\bar{9}$ 1 5

shaken, centrifuged, filtered and the absorbance of the resulting green blue solution (ABTS free radical solution) at 734 nm was adjusted to ca. 0.5. Then, 50 μL of (2 mM) solution of the tested compound in spectroscopic grade CH_3OH /phosphate buffer (1:1) was added. The absorbance was measured and the reduction in color intensity was expressed as inhibition percentage (1%). Blank sample was run without ABTS and using CH_3OH /phosphate buffer (1:1) instead of tested compounds. L-Ascorbic acid was used as standard antioxidant (positive control) and the negative control was run with ABTS and CH_3OH /phosphate buffer (1:1) only. The inhibition percentage was calculated by Eq. (5):

$$\% \text{Inhibition} = \frac{A(\text{control}) - A(\text{test})}{A(\text{control})} \times 100 \quad (5)$$

3. Results and discussion

The results of physical properties of the prepared ligands (HL_n) and their Cu(II) complexes (**1–3**) along with their elemental analysis are collected in Table 1. All the complexes show 1:1 metal-ligand stereochemistry. They are stable in air and soluble in most common organic solvents. The molar conductance in DMF (10^{-3} M) at room temperature reveal the non-electrolytic nature of Cu(II) complexes [29,30].

3.1. IR spectra

The FT-IR spectra of Cu(II) complexes (**1–3**) show significant changes as compared to the spectra obtained for the corresponding

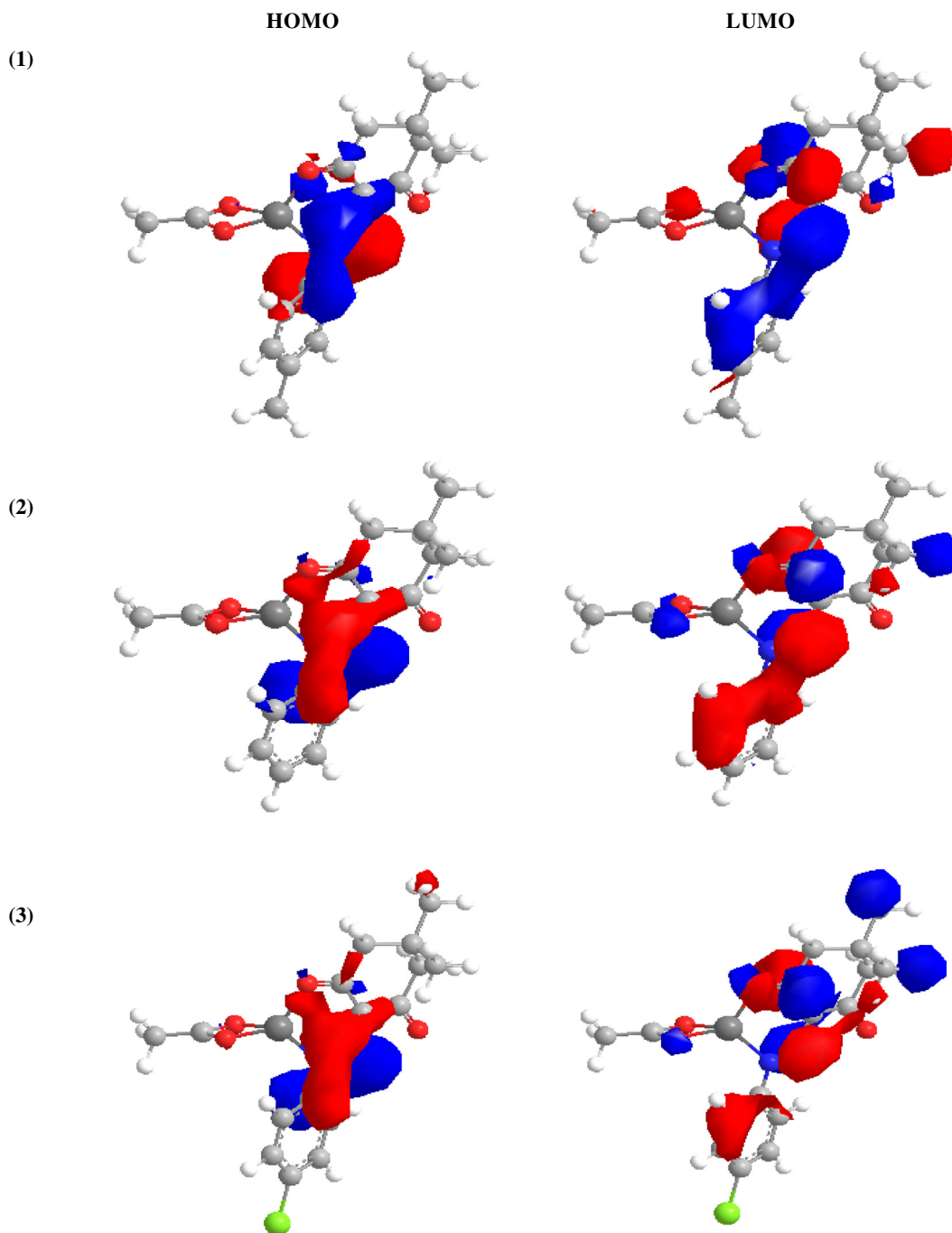


Fig. 4. The highest occupied Molecular orbital (HOMO) and the lowest unoccupied molecular orbital (LUMO) of Cu(II) complexes (**1–3**).

ligands (**HL_n**). The ligands can exist as a mixture of different keto-enol tautomers which deprotonate and bind to the Cu as a monomeric bidentate ligands. The following features can be pointed out:

1. In the spectra of the ligands a broad band of $\nu(\text{NH})$ group which corresponding to H-bonded hydrazone structure appeared at $2935\text{--}2952\text{ cm}^{-1}$ region, was disappeared in Cu(II) complexes indicating that the ligands are coordinated in the deprotonated hydrazone form [18,31].
2. The bands due to $\nu(\text{C}=\text{O free})$ and $\nu(\text{C}=\text{O}\cdots\text{H})$ groups appeared in the spectra of the ligands at $1671\text{--}1673$ and $1617\text{--}1623\text{ cm}^{-1}$ regions, respectively [32]. The band of $\nu(\text{C}=\text{O free})$ was shifted to lower wavenumber by $8\text{--}12\text{ cm}^{-1}$ indicating their coordination to the Cu center. The observed hypsochromic shift in the IR wavenumbers of Cu(II) complexes can be related to a strengthening of the strong intramolecular resonance assisted hydrogen bond in the complexes in contrast to the free ligands [19,32]. However, experimentally it was found that the studied ligands are stabilized in the hydrazo form with formation of a hydrogen bond between the

hydrazone = N—NH— moiety and a carbonyl group giving a six-membered ring.

3. Spectra of the ligands display a band at $1510\text{--}1519\text{ cm}^{-1}$ range due to $\nu(\text{C}=\text{N})$ without a noticeable change from that of Cu(II) complexes suggesting a non-bonding nature of the nitrogen atom of (C=N) group to Cu(II) ions [33].
4. The IR spectra of $[\text{Cu}(\text{L}_n)(\text{CH}_3\text{COO})]\text{XH}_2\text{O}$ complexes shows two strong at $1455\text{--}1460$ and $1317\text{--}1328\text{ cm}^{-1}$ regions which were assigned to $\nu_{\text{asym}}(\text{COO}^-)$ and $\nu_{\text{sym}}(\text{COO}^-)$ stretches of coordinated carboxylate group, respectively [34]. The average $\Delta\nu = \nu_{\text{asym}} - \nu_{\text{sym}} = 125\text{--}135\text{ cm}^{-1}$ indicating bidentate coordination of carboxylate [35]. Coordination via oxygen of carboxylate is confirmed by $\nu(\text{Cu}—\text{O})$ band at $518\text{--}530\text{ cm}^{-1}$ region. Thus, Cu(II) complexes are coordinated through oxygen of carboxylates.
5. The presence of lattice coordinated water molecules in the structure of Cu(II) complexes is further supported by the appearance of the broad band at $3453\text{--}3460\text{ cm}^{-1}$ region corresponding to $\nu(\text{OH})$ of water molecules [36]. The nature of water of crystallization will be discussed in the thermal analysis part.

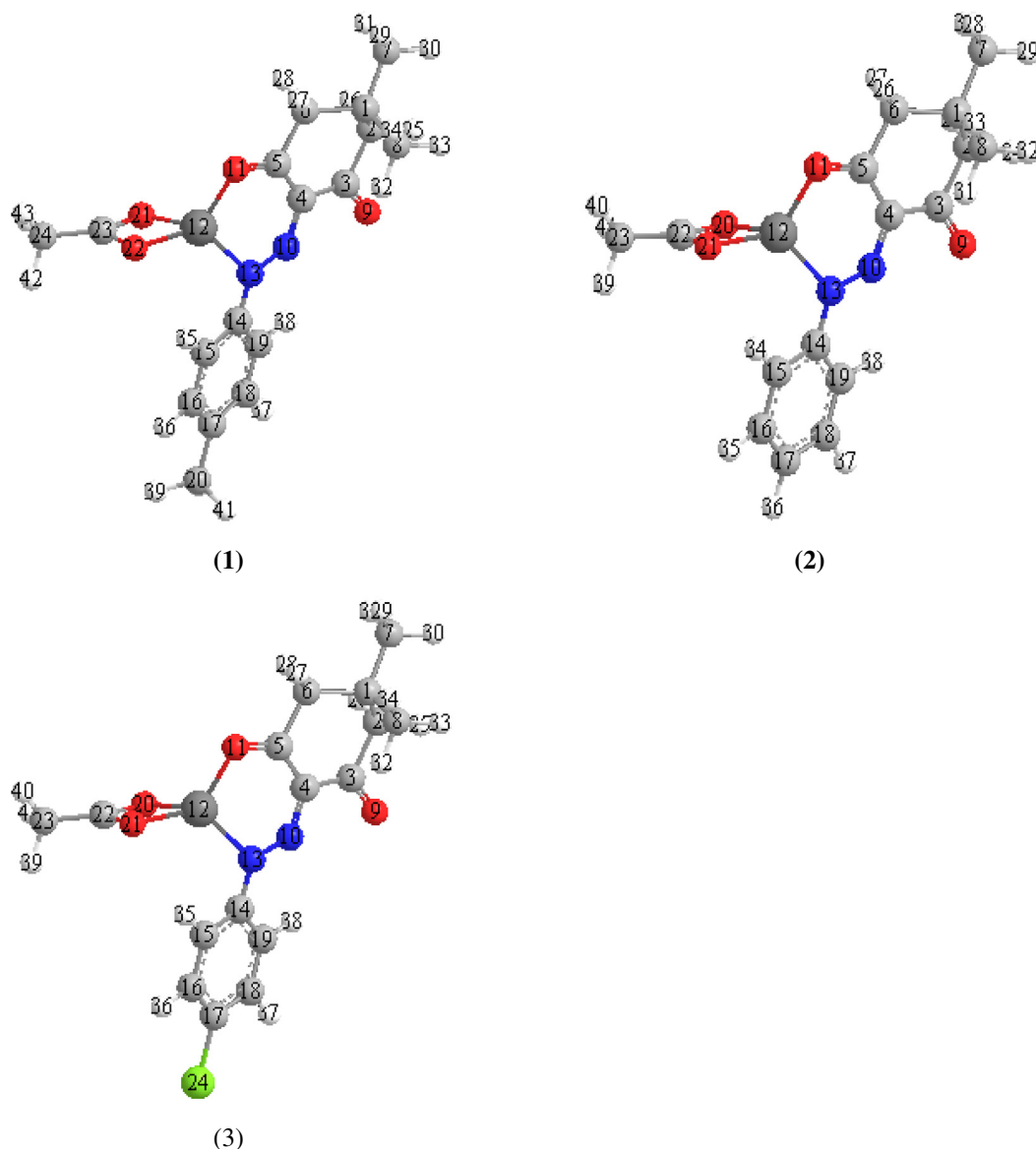


Fig. 5. The calculated molecular structures of Cu(II) complexes (1–3).

6. In addition, new bands were observed in the regions 518–530 and 455–468 cm^{-1} which were assigned to the formation of Cu ← O and Cu—N bonds, respectively [37]. This further supports the coordination of the oxygen atom of the free C=O group and nitrogen atom of the hydrazone structure (NH) with deportation.
7. The peaks between 3030 and 3058 cm^{-1} in the spectra of the ligands and their Cu(II) complexes are due to $\nu(\text{CH}_{\text{arom}})$ stretching [33].

3.2. Magnetic moments and electronic spectra

The observed magnetic moment of Cu(II) complexes (**1–3**) lie in the range 1.72–1.76 B.M. at room temperature (Table 1) indicates the non-coupled mononuclear complexes of magnetically diluted d^9 system with $S = 1/2$ spin-state [38]. The μ_{eff} values of mononuclear Cu(II) complexes are normal within range reported for one unpaired electron in square planar structure. The electronic spectra of free ligands (**HL_n**) and their Cu(II) complexes are recorded in 10^{-5} DMF solution in the wavelength range 200–800 nm. The free ligands exhibit two intense

bands in 38,760–37,735 and 25,000–24,213 cm^{-1} region due to $\pi \rightarrow \pi^*$ transitions of the aromatic ring and $n \rightarrow \pi^*$ transitions of the C=O and C=N group, respectively [38]. These peaks exhibited bathochromic shift upon complex formation, which supported the coordination of the ligands to Cu(II) ion. The electronic spectra of Cu(II) complexes (**1–3**) show a broad band at 27027–25773 cm^{-1} region, which is assigned to d-d (${}^2B_{1g} \rightarrow {}^2A_{1g}$) transition. From the above electronic spectral data and magnetic moment values, it is concluded that the Cu(II) complexes exhibit a square planar geometry around the metal ion [31].

3.3. ${}^1\text{H}$ NMR and ${}^{13}\text{C}$ NMR spectra

The ${}^1\text{H}$ NMR and ${}^{13}\text{C}$ NMR spectra of a mixture of enol-azo and hydrazone tautomers of the ligands (**HL_n**) were recorded in DMSO- d_6 at room temperature. ${}^1\text{H}$ NMR (300 MHz) in DMSO- d_6 , internal TMS, the hydrazone proton (—C=N—NH—) shows a singlet at δ 14.1–14.7 ppm region for the ligands (**HL_n**) are in agreement with the literature [18,32]. This signal disappeared when a D_2O exchange

Table 3
The bond lengths and bond angles of Cu(II) complex (**1**).

Bond lengths (Å)		Bond angles (°)		Bond angles (°)	
C(20)—H(40)	1.113	H(44)—C(24)—H(43)	108.932	H(31)—C(7)—H(30)	107.413
C(20)—H(39)	1.113	H(44)—C(24)—H(42)	108.911	H(31)—C(7)—H(29)	107.465
C(19)—H(38)	1.103	H(44)—C(24)—C(23)	109.935	H(31)—C(7)—C(1)	111.679
C(18)—H(37)	1.103	H(43)—C(24)—H(42)	109.220	H(30)—C(7)—H(29)	107.702
C(16)—H(36)	1.103	H(43)—C(24)—C(23)	109.936	H(30)—C(7)—C(1)	111.186
C(15)—H(35)	1.102	H(42)—C(24)—C(23)	109.883	H(29)—C(7)—C(1)	111.191
C(8)—H(34)	1.113	C(24)—C(23)—O(22)	122.068	H(28)—C(6)—H(27)	106.687
C(8)—H(33)	1.113	C(24)—C(23)—O(21)	144.715	H(28)—C(6)—C(1)	110.059
C(8)—H(32)	1.112	O(22)—C(23)—O(21)	93.216	H(28)—C(6)—C(5)	106.345
C(7)—H(31)	1.113	Cu(12)—O(22)—C(23)	93.991	H(27)—C(6)—C(1)	108.330
C(7)—H(30)	1.114	Cu(12)—O(21)—C(23)	107.149	H(27)—C(6)—C(5)	109.980
C(7)—H(29)	1.114	H(41)—C(20)—H(40)	108.276	C(1)—C(6)—C(5)	115.121
C(6)—H(28)	1.116	H(41)—C(20)—H(39)	108.311	O(11)—C(5)—C(6)	111.221
C(6)—H(27)	1.116	H(41)—C(20)—C(17)	109.830	O(11)—C(5)—C(4)	129.648
C(2)—H(26)	1.115	H(40)—C(20)—H(39)	106.896	C(6)—C(5)—C(4)	119.079
C(2)—H(25)	1.115	H(40)—C(20)—C(17)	111.778	N(10)—C(4)—C(5)	126.114
C(14)—C(19)	1.350	H(39)—C(20)—C(17)	111.608	N(10)—C(4)—C(3)	112.810
C(18)—C(19)	1.342	H(38)—C(19)—C(14)	121.738	C(5)—C(4)—C(3)	121.062
C(17)—C(18)	1.342	H(38)—C(19)—C(18)	116.075	O(9)—C(3)—C(4)	124.372
C(16)—C(17)	1.342	C(14)—C(19)—C(18)	122.183	O(9)—C(3)—C(2)	115.120
C(15)—C(16)	1.342	H(37)—C(18)—C(19)	119.374	C(4)—C(3)—C(2)	120.498
C(14)—C(15)	1.349	H(37)—C(18)—C(17)	119.500	H(26)—C(2)—H(25)	107.024
N(13)—Cu(12)	1.840	C(19)—C(18)—C(17)	121.125	H(26)—C(2)—C(3)	107.353
Cu(12)—O(22)	1.834	C(18)—C(17)—C(16)	117.487	H(26)—C(2)—C(1)	111.046
O(21)—Cu(12)	1.801	C(18)—C(17)—C(20)	121.316	H(25)—C(2)—C(3)	110.199
O(11)—Cu(12)	1.810	C(16)—C(17)—C(20)	121.197	H(25)—C(2)—C(1)	108.787
C(23)—C(24)	1.493	H(36)—C(16)—C(17)	119.504	C(3)—C(2)—C(1)	112.299
O(22)—C(23)	1.493	H(36)—C(16)—C(15)	119.426	C(8)—C(1)—C(7)	108.907
O(21)—C(23)	1.205	C(17)—C(16)—C(15)	121.065	C(8)—C(1)—C(6)	110.899
C(17)—C(20)	1.510	H(35)—C(15)—C(16)	116.123	C(8)—C(1)—C(2)	111.152
N(13)—C(14)	1.282	H(35)—C(15)—C(14)	121.580	C(7)—C(1)—C(6)	110.402
N(10)—N(13)	1.241	C(16)—C(15)—C(14)	122.281	C(7)—C(1)—C(2)	110.266
C(5)—O(11)	1.238	C(19)—C(14)—C(15)	115.839	C(6)—C(1)—C(2)	105.188
C(4)—N(10)	1.279	C(19)—C(14)—N(13)	122.094		
C(3)—O(9)	1.218	C(15)—C(14)—N(13)	122.041		
C(1)—C(8)	1.542	Cu(12)—N(13)—C(14)	120.851		
C(1)—C(7)	1.541	Cu(12)—N(13)—N(10)	109.633		
C(6)—C(1)	1.530	C(14)—N(13)—N(10)	122.576		
C(5)—C(6)	1.531	N(13)—Cu(12)—O(22)	125.502		
C(4)—C(5)	1.380	N(13)—Cu(12)—O(21)	116.192		
C(3)—C(4)	1.376	N(13)—Cu(12)—O(11)	105.251		
C(2)—C(3)	1.522	O(22)—Cu(12)—O(21)	65.643		
C(1)—C(2)	1.529	O(22)—Cu(12)—O(11)	122.470		
		O(21)—Cu(12)—O(11)	116.815		
		Cu(12)—O(11)—C(5)	109.938		
		N(13)—N(10)—C(4)	128.502		
		H(34)—C(8)—H(33)	107.499		
		H(34)—C(8)—H(32)	107.079		
		H(34)—C(8)—C(1)	111.109		
		H(33)—C(8)—H(32)	107.288		
		H(33)—C(8)—C(1)	111.093		
		H(32)—C(8)—C(1)	112.520		

experiment was carried out [39]. δ (ppm) = 0.98 (s, 3H, CH₃), 1.33 (s, 3H, CH₃), 3.35 (s, 4H, 2CH₂), 7.20–7.85 (s, 4H, Ar–H), 14.25 (s, 1H, NH). ¹³C{¹H} NMR (75 MHz) in DMSO-*d*₆, internal TMS, δ (ppm):

- (HL₁) δ = 22.4 (CH₃), 26.3 (CH₃), 52.3 (2CH₂), 118.6 (Ar–H), 120.6 (Ar–H), 134.1 (C=N), 138.9 (Ar–NH–N), 193.2 (C=O), 197.2 (C=O).
- (HL₂) δ = 26.5 (CH₃), 30.8 (CH₃), 52.2 (2CH₂), 119.0 (Ar–H), 126.7 (Ar–H), 129.7 (C=N), 141.7 (Ar–NH–N), 191.8 (C=O), 196.1 (C=O).
- (HL₃) δ = 26.7 (CH₃), 28.7 (CH₃), 53.1 (2CH₂), 119.4 (Ar–H), 121.8 (Ar–H), 133.7 (C=N), 139.3 (Ar–NH–N), 192.0 (C=O), 197.2 (C=O).

3.4. X-ray diffraction

The X-ray diffraction (XRD) patterns of Cu(II) complex (2) was presented in Fig. 3.

It shows many diffraction peaks which indicate that Cu(II) complex (2) is a polycrystalline with monoclinic crystal system and structure with space group *p*21/*M*.

The average crystallite size (ξ) and The dislocation density (δ) can be calculated from the XRD pattern according to following Eqs. (6) and (7) [40–41].

$$\xi = \frac{0.95\lambda}{\beta_{1/2} \cos\theta}, \quad (6)$$

$$\delta = \frac{1}{D^2} \quad (7)$$

where λ is the wavelength of X-ray radiation ($\lambda = 1.54060 \text{ \AA}$), $\beta_{1/2}$ is full width at half maximum of the reference diffraction peak measured in radians and θ is the angle of diffraction. The calculated value of ξ and δ was found to be 61 nm and $2.69 \times 10^{-4} \text{ nm}^{-2}$. The calculated lattice parameters (*a*, *b*, *c*, α , β and γ), inter-planar spacing, *d*, and Miller indices *hkl*, of Cu(II) complex (2) are listed in Table 2.

Table 4
The bond lengths and bond angles of Cu(II) complex (2).

Bond lengths (Å)		Bond angles (°)		Bond angles (°)	
C(23)–H(41)	1.113	H(41)–C(23)–H(40)	108.928	H(29)–C(7)–C(1)	111.185
C(23)–H(40)	1.113	H(41)–C(23)–H(39)	108.905	H(28)–C(7)–C(1)	111.195
C(23)–H(39)	1.113	H(41)–C(23)–C(22)	109.941	H(27)–C(6)–H(26)	106.681
C(19)–H(38)	1.103	H(40)–C(23)–H(39)	109.210	H(27)–C(6)–C(1)	110.075
C(18)–H(37)	1.103	H(40)–C(23)–C(22)	109.940	H(27)–C(6)–C(5)	106.363
C(17)–H(36)	1.103	H(39)–C(23)–C(22)	109.891	H(26)–C(6)–C(1)	108.334
C(16)–H(35)	1.103	C(23)–C(22)–O(21)	122.063	H(26)–C(6)–C(5)	109.983
C(15)–H(34)	1.102	C(23)–C(22)–O(20)	144.717	C(1)–C(6)–C(5)	115.088
C(8)–H(33)	1.113	O(21)–C(22)–O(20)	93.219	O(11)–C(5)–C(6)	111.218
C(8)–H(32)	1.113	Cu(12)–O(21)–C(22)	93.986	O(11)–C(5)–C(4)	129.666
C(8)–H(31)	1.112	Cu(12)–O(20)–C(22)	107.149	C(6)–C(5)–C(4)	119.068
C(7)–H(30)	1.113	H(38)–C(19)–C(14)	121.824	N(10)–C(4)–C(5)	126.113
C(7)–H(29)	1.114	H(38)–C(19)–C(18)	115.983	N(10)–C(4)–C(3)	112.800
C(7)–H(28)	1.114	C(14)–C(19)–C(18)	122.189	C(5)–C(4)–C(3)	121.072
C(6)–H(27)	1.116	H(37)–C(18)–C(19)	120.142	O(9)–C(3)–C(4)	124.354
C(6)–H(26)	1.116	H(37)–C(18)–C(17)	119.605	O(9)–C(3)–C(2)	115.117
C(2)–H(25)	1.115	C(19)–C(18)–C(17)	120.253	C(4)–C(3)–C(2)	120.518
C(2)–H(24)	1.115	H(36)–C(17)–C(18)	120.540	H(25)–C(2)–H(24)	107.024
C(14)–C(19)	1.351	H(36)–C(17)–C(16)	120.535	H(25)–C(2)–C(3)	107.334
C(18)–C(19)	1.343	C(18)–C(17)–C(16)	118.920	H(25)–C(2)–C(1)	111.039
C(17)–C(18)	1.340	H(35)–C(16)–C(17)	119.655	H(24)–C(2)–C(3)	110.188
C(16)–C(17)	1.340	H(35)–C(16)–C(15)	120.153	H(24)–C(2)–C(1)	108.783
C(15)–C(16)	1.343	C(17)–C(16)–C(15)	120.187	C(3)–C(2)–C(1)	112.338
C(14)–C(15)	1.350	H(34)–C(15)–C(16)	116.060	C(8)–C(1)–C(7)	116.909
N(13)–Cu(12)	1.840	H(34)–C(15)–C(14)	121.634	C(8)–C(1)–C(6)	110.895
Cu(12)–O(21)	1.834	C(16)–C(15)–C(14)	122.290	C(8)–C(1)–C(2)	111.153
O(20)–Cu(12)	1.801	C(19)–C(14)–C(15)	116.138	C(7)–C(1)–C(6)	110.402
O(11)–Cu(12)	1.810	C(19)–C(14)–N(13)	121.962	C(7)–C(1)–C(2)	110.263
C(22)–C(23)	1.493	C(15)–C(14)–N(13)	121.873	C(6)–C(1)–C(2)	105.190
O(21)–C(22)	1.493	Cu(12)–N(13)–C(14)	120.864	H(29)–C(7)–C(1)	111.185
O(20)–C(22)	1.205	Cu(12)–N(13)–N(10)	109.622	H(28)–C(7)–C(1)	111.195
N(13)–C(14)	1.282	C(14)–N(13)–N(10)	122.549	H(27)–C(6)–H(26)	106.681
N(10)–N(13)	1.241	N(13)–Cu(12)–O(21)	125.443	H(27)–C(6)–C(1)	110.075
C(5)–O(11)	1.238	N(13)–Cu(12)–O(20)	116.330	H(27)–C(6)–C(5)	106.363
C(4)–N(10)	1.279	N(13)–Cu(12)–O(11)	105.315	H(26)–C(6)–C(1)	108.334
C(3)–O(9)	1.218	O(21)–Cu(12)–O(20)	65.645	H(26)–C(6)–C(5)	109.983
C(1)–C(8)	1.542	O(21)–Cu(12)–O(11)	122.274	C(1)–C(6)–C(5)	115.088
C(1)–C(7)	1.541	O(20)–Cu(12)–O(11)	116.952	O(11)–C(5)–C(6)	111.218
C(6)–C(1)	1.530	Cu(12)–O(11)–C(5)	109.942	O(11)–C(5)–C(4)	129.666
C(5)–C(6)	1.531	N(13)–N(10)–C(4)	128.549		
C(4)–C(5)	1.380	H(33)–C(8)–H(32)	107.504		
C(3)–C(4)	1.376	H(33)–C(8)–H(31)	107.080		
C(2)–C(3)	1.522	H(33)–C(8)–C(1)	111.111		
C(1)–C(2)	1.529	H(32)–C(8)–H(31)	107.289		
		H(32)–C(8)–C(1)	111.089		
		H(31)–C(8)–C(1)	112.514		
		H(30)–C(7)–H(29)	107.411		
		H(30)–C(7)–H(28)	107.463		
		H(30)–C(7)–C(1)	111.680		
		H(29)–C(7)–H(28)	107.702		

Table 5
The bond lengths and bond angles of Cu(II) complex (3).

Bond lengths (Å)		Bond angles (°)		Bond angles (°)	
C(23)–H(41)	1.113	H(41)–C(23)–H(40)	108.939	H(28)–C(6)–C(5)	106.348
C(23)–H(40)	1.113	H(41)–C(23)–H(39)	108.906	H(27)–C(6)–C(5)	109.976
C(23)–H(39)	1.113	H(41)–C(23)–C(22)	109.935	H(27)–C(6)–C(1)	108.344
C(19)–H(38)	1.103	H(40)–C(23)–H(39)	109.213	C(5)–C(6)–C(1)	115.113
C(18)–H(37)	1.103	H(40)–C(23)–C(22)	109.941	O(11)–C(5)–C(6)	111.239
C(16)–H(36)	1.103	H(39)–C(23)–C(22)	109.882	O(11)–C(5)–C(4)	129.638
C(15)–H(35)	1.102	C(23)–C(22)–O(21)	122.071	C(6)–C(5)–C(4)	119.073
C(8)–H(34)	1.113	C(23)–C(22)–O(20)	144.715	N(10)–C(4)–C(5)	126.120
C(8)–H(33)	1.113	O(21)–C(22)–O(20)	93.213	N(10)–C(4)–C(3)	112.788
C(8)–H(32)	1.112	C(22)–O(21)–Cu(12)	93.990	C(5)–C(4)–C(3)	121.077
C(7)–H(31)	1.113	C(22)–O(20)–Cu(12)	107.152	O(9)–C(3)–C(4)	124.300
C(7)–H(30)	1.114	H(38)–C(19)–C(18)	115.965	O(9)–C(3)–C(2)	115.184
C(7)–H(29)	1.114	H(38)–C(19)–C(14)	121.736	C(4)–C(3)–C(2)	120.506
C(6)–H(28)	1.116	C(18)–C(19)–C(14)	122.294	H(26)–C(2)–H(25)	107.032
C(6)–H(27)	1.116	H(37)–C(18)–C(19)	119.476	H(26)–C(2)–C(3)	107.342
C(2)–H(26)	1.115	H(37)–C(18)–C(17)	120.438	H(26)–C(2)–C(1)	111.047
C(2)–H(25)	1.115	C(19)–C(18)–C(17)	120.086	H(25)–C(2)–C(3)	110.185
C(14)–C(19)	1.351	Cl(24)–C(17)–C(18)	120.517	H(25)–C(2)–C(1)	108.799
C(18)–C(19)	1.343	Cl(24)–C(17)–C(16)	120.405	C(3)–C(2)–C(1)	112.302
C(17)–C(18)	1.340	C(18)–C(17)–C(16)	119.075	C(8)–C(1)–C(7)	108.908
C(16)–C(17)	1.340	H(36)–C(16)–C(17)	120.493	C(8)–C(1)–C(6)	110.894
C(15)–C(16)	1.343	H(36)–C(16)–C(15)	119.461	C(8)–C(1)–C(2)	111.146
C(14)–C(15)	1.350	C(17)–C(16)–C(15)	120.042	C(7)–C(1)–C(6)	110.400
C(17)–Cl(24)	1.726	H(35)–C(15)–C(16)	116.071	C(7)–C(1)–C(2)	110.259
N(13)–Cu(12)	1.840	H(35)–C(15)–C(14)	121.538	C(6)–C(1)–C(2)	105.207
Cu(12)–O(21)	1.834	C(16)–C(15)–C(14)	122.376		
O(20)–Cu(12)	1.801	C(19)–C(14)–C(15)	116.104		
O(11)–Cu(12)	1.810	C(19)–C(14)–N(13)	122.007		
C(22)–C(23)	1.493	C(15)–C(14)–N(13)	121.863		
O(21)–C(22)	1.493	C(14)–N(13)–Cu(12)	120.829		
O(20)–C(22)	1.205	C(14)–N(13)–N(10)	122.527		
N(13)–C(14)	1.282	Cu(12)–N(13)–N(10)	109.591		
N(10)–N(13)	1.241	O(21)–Cu(12)–O(20)	65.642		
C(5)–O(11)	1.238	O(21)–Cu(12)–N(13)	125.549		
C(4)–N(10)	1.279	O(21)–Cu(12)–O(11)	122.325		
C(3)–O(9)	1.218	O(20)–Cu(12)–N(13)	116.116		
C(1)–C(8)	1.542	O(20)–Cu(12)–O(11)	116.918		
C(1)–C(7)	1.541	N(13)–Cu(12)–O(11)	105.316		
C(6)–C(1)	1.530	Cu(12)–O(11)–C(5)	109.943		
C(5)–C(6)	1.531	N(13)–N(10)–C(4)	128.566		
C(4)–C(5)	1.380	H(34)–C(8)–H(33)	107.499		
C(3)–C(4)	1.376	H(34)–C(8)–H(32)	107.079		
C(2)–C(3)	1.522	H(34)–C(8)–C(1)	111.115		
C(1)–C(2)	1.529	H(33)–C(8)–H(32)	107.291		
		H(33)–C(8)–C(1)	111.089		
		H(32)–C(8)–C(1)	112.516		
		H(31)–C(7)–H(30)	107.412		
		H(31)–C(7)–H(29)	107.464		
		H(31)–C(7)–C(1)	111.679		
		H(30)–C(7)–H(29)	107.702		
		H(30)–C(7)–C(1)	111.185		
		H(29)–C(7)–C(1)	111.194		
		H(28)–C(6)–H(27)	106.679		
		H(28)–C(6)–C(1)	110.061		

3.5. Molecular structure

The molecular structures (HOMO & LUMO) of Cu(II) complexes (1–3) are presented in Figs. 4 and 5 and the selected geometric parameters bond lengths and bond angles are listed in Tables 3–5. The calculated quantum chemical parameters are given in Table 6. The HOMO–LUMO

energy gap (ΔE) is an important stability index which is applied to develop theoretical models for explaining the structure and conformation barriers in many molecular systems. From the values of ΔE of Cu(II) complexes indicate that the complex (2) more stable than the other complexes. Additional parameters such as separation energies, ΔE , absolute electronegativities, χ , chemical potentials, Π , absolute hardness,

Table 6
The calculated quantum chemical properties of Cu(II) complexes (1–3).

Compound	$-E_{\text{HOMO}}$ (a.u.)	$-E_{\text{LUMO}}$ (a.u.)	ΔE (a.u.)	χ (a.u.)	η (a.u.)	σ (a.u.) ⁻¹	$-\Pi$ (a.u.)	S (a.u.) ⁻¹	ω (a.u.)	ΔN_{max} (a.u.)
(1)	4.595	2.745	1.850	3.670	0.925	1.081	3.670	0.541	7.280	3.968
(2)	4.609	2.863	1.746	3.736	0.873	1.145	3.736	0.573	7.994	4.279
(3)	4.565	2.526	2.039	3.546	1.020	0.981	3.546	0.490	6.165	3.478

η , absolute softness, σ , global electrophilicity, ω , global softness, S and additional electronic charge, ΔN_{\max} , have been calculated according to the following Eqs. (8)–(15) [42]:

$$\Delta E = E_{LUMO} - E_{HOMO} \quad (8)$$

$$\chi = \frac{-(E_{HOMO} + E_{LUMO})}{2} \quad (9)$$

$$\eta = \frac{E_{LUMO} - E_{HOMO}}{2} \quad (10)$$

$$\sigma = 1/\eta \quad (11)$$

$$Pi = -\chi \quad (12)$$

$$S = \frac{1}{2\eta} \quad (13)$$

$$\omega = Pi^2/2\eta \quad (14)$$

$$\Delta N_{\max} = -Pi/\eta \quad (15)$$

3.6. Thermal analyses

The thermal properties of ligands (**HL_n**) and their Cu(II) complexes (**1–3**) were characterized on the basis of thermogravimetric analysis (TGA). The temperature intervals and the percentage of loss of masses of the ligands and their Cu(II) complexes are listed in Table 7. It is clear that the change of substituent affects the thermal properties of the ligands.

All Cu(II) complexes (**1–3**) showed TG curves in the temperature range ~100–210 °C loss of CH₃COO[−] and H₂O molecules. The second stage is related to loss of the part of ligand. The final weight losses are due to the decomposition of the rest of the carbon atoms and CuO residue.

3.7. Calculation of activation thermodynamic parameters

The thermodynamic activation parameters of decomposition processes of the ligands (**HL_n**) and their Cu(II) complexes (**1–3**) namely activation energy (E_a), enthalpy (ΔH^*), entropy (ΔS^*), and Gibbs free energy change of the decomposition (ΔG^*) are evaluated graphically by employing the Coast-Redfern [43] and Horowitz-Metzger [44] methods.

3.7.1. Coast-Redfern equation

The Coast-Redfern equation, which is a typical integral method, can represent as:

$$\int_0^a \frac{dx}{(1-\alpha)^n} = \frac{A}{\varphi} \int_{T_1}^{T_2} \exp\left(-\frac{E_a}{RT}\right) dt \quad (16)$$

For convenience of integration, the lower limit T_1 usually taken as zero. This equation on integration gives:

$$\ln\left[-\frac{\ln(1-\alpha)}{T^2}\right] = -\frac{E_a}{RT} + \ln\left[\frac{AR}{\varphi E_a}\right] \quad (17)$$

A plot of left-hand side (LHS) against $1/T$ was drawn (Fig. 6). E_a is the energy of activation in kJ/mol and calculated from the slope and A in (s^{−1}) from the intercept value. The entropy of activation (ΔS^*) in (J mol^{−1} K^{−1}) calculated by using the equation:

$$\Delta S^* = 2.303 \left[\log\left(\frac{Ah}{k_B T_s}\right) \right] R \quad (18)$$

where k_B is the Boltzmann constant, h is the Planck's constant and T_s is the TG peak temperature.

3.7.2. Horowitz-Metzger equation

The Horowitz-Metzger equation is an illustrative of the approximation methods. These authors derived the relation:

$$\log\left[\frac{(1-(1-\alpha)^{1-n})}{(1-n)}\right] = \frac{E_a \theta}{2.303RT_s^2}, \quad (19)$$

for $n \neq 1$

when $n = 1$, the LHS of Eq. (18) would be $\log[-\log(1-\alpha)]$ (Fig. 7). For a first order kinetic process, the Horowitz-Metzger equation may write in the form:

$$\log\left[\log\left(\frac{w_\alpha}{w_\gamma}\right)\right] = \frac{E_a \theta}{2.303RT_s^2} - \log 2.303 \quad (20)$$

where $\theta = T - T_s$, $w_\gamma = w_\alpha - w$, w_α = mass loss at the completion reaction; w = mass loss up to time t . The plot of $\log[\log(w_\alpha/w_\gamma)]$ vs. θ was drawn and found to be linear from the slope of which E_a was calculated. The pre-exponential factor, A , calculated from equation:

$$\frac{E_a}{RT_s^2} = \frac{A}{\left[\varphi \exp\left(-\frac{E_a}{RT_s}\right)\right]} \quad (21)$$

The entropy of activation, ΔS^* , is calculated from Eq. (18). The enthalpy activation, ΔH^* , and Gibbs free energy, ΔG^* , calculated from:

$$\Delta H^* = E_a - RT \quad (22)$$

$$\Delta G^* = \Delta H^* - T\Delta S^* \quad (23)$$

The calculated values of E_a , A , ΔS^* , ΔH^* and ΔG^* for the decomposition steps for ligands (**HL₁**, **HL₂** and **HL₃**) and their Cu(II) complexes (**1–3**) are summarized in Table 8.

3.8. DNA binding studies

DNA is the classical pharmacological target of metal-based anticancer agents; therefore, the study of the potential interaction of

Table 7
Thermal analysis data for the ligands (**HL_n**) and their Cu(II) complexes (**1–3**).

Compound ^a	Temp. range (°C)	Found mass loss (calc.) %	Assignment
HL₁	120–270	68.22 (69.37)	Loss of C ₉ H ₁₁ O ₂ N ₂
	270–510	27.78 (25.99)	Loss of C ₅ H ₇
	>600	4.0 (4.65)	Loss of carbon atoms
HL₂	120–27	92.27 (90.05)	Loss of C ₁₂ H ₁₆ O ₂ N ₂
	270–540	4.53 (4.91)	Loss of C atom
	>600	2.43 (2.45)	Loss of C atom
HL₃	150–270	90.96 (91.38)	Loss of C ₁₂ H ₁₅ N ₂ O ₂ Cl
	270–510	5.34 (6.46)	Loss of C atom
	>600	3.7 (2.15)	Loss of C atom
(1)	92–180	8 (8.66)	Loss of 2H ₂ O
	180–330	33.48 (33.22)	Loss of CH ₃ COO + C ₆ H ₇
	330–420	34.18 (33.46)	Loss of C ₇ H ₁₁ N ₂ O
	>800	24.34 (24.9)	Loss of carbon atoms + CuO
(2)	120–390	40.29 (40.77)	Loss of CH ₃ COO + C ₇ H ₆
	390–510	39.62 (37.49)	Loss of C ₇ H ₉ N ₂ O
	>800	20.1 (21.74)	Loss of carbon atoms + CuO
(3)	107–210	3.67 (4.31)	Loss of H ₂ O
	210–30	29.4 (29.43)	Loss of CH ₃ COO + C ₅ H ₄
	300–43	6.61 (6.70)	Loss of C ₂ H ₄
	435–615	40.29 (37.91)	Loss of C ₆ H ₇ N ₂ OCl
	>800	20.03 (21.89)	Loss of carbon atoms + CuO

^a Numbers as given in Table 1.

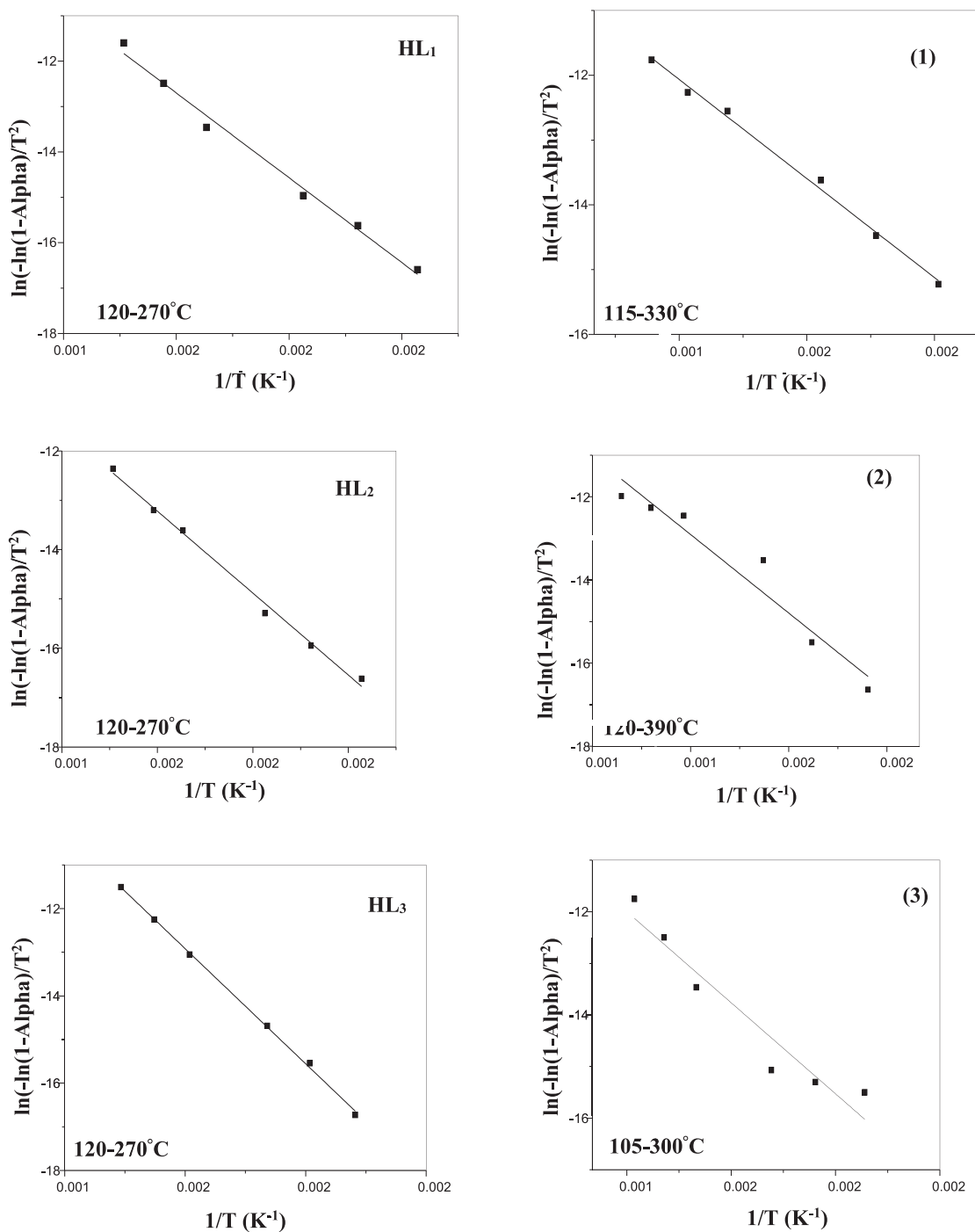


Fig. 6. Coats-Redfern (CR) of the ligands (HL_n) and their Cu(II) complexes (1-3).

coordination compounds with DNA is of paramount importance for the development of molecules with potential medical applications. There are four possible ways in which small molecules can bind to double-stranded DNA; (i) intercalation between two adjacent base pairs and perpendicular to the helical axis; (ii) outside-edge binding to the sugar-phosphate backbone of the helix through electrostatic interactions; (iii) groove binding with functional groups into either the major or minor groove [45] and (iv) the covalent interaction between DNA and metal complexes at the nitrogen atoms of nucleobases. Therefore, several characterization techniques have been employed to study the interactions of ligands (HL_n) and their copper(II) complexes (1-3) with CT-DNA.

3.8.1. Electronic absorption titrations

Electronic absorption spectroscopy is an effective method to examine the binding mode and extent of ligands (HL_n) and their metal complexes (1-3) with DNA [46]. We have determined the intrinsic binding constant to CT-DNA by monitoring the absorption intensity of the charge transfer spectral bands near 413, 400 and 406 nm for the ligands HL₁, HL₂ and HL₃, respectively and 410, 399 and 395 nm for Cu(II) complexes (1, 2 and 3), respectively. Upon the addition of increasing amount of CT-DNA, a significant "hyperchromic" effect was observed accompanied by a moderate red shift of 2–3 nm, indicative of stabilization of the DNA helix. These spectral characteristics suggest that the ligands and complexes bind either to the external contact (electrostatic

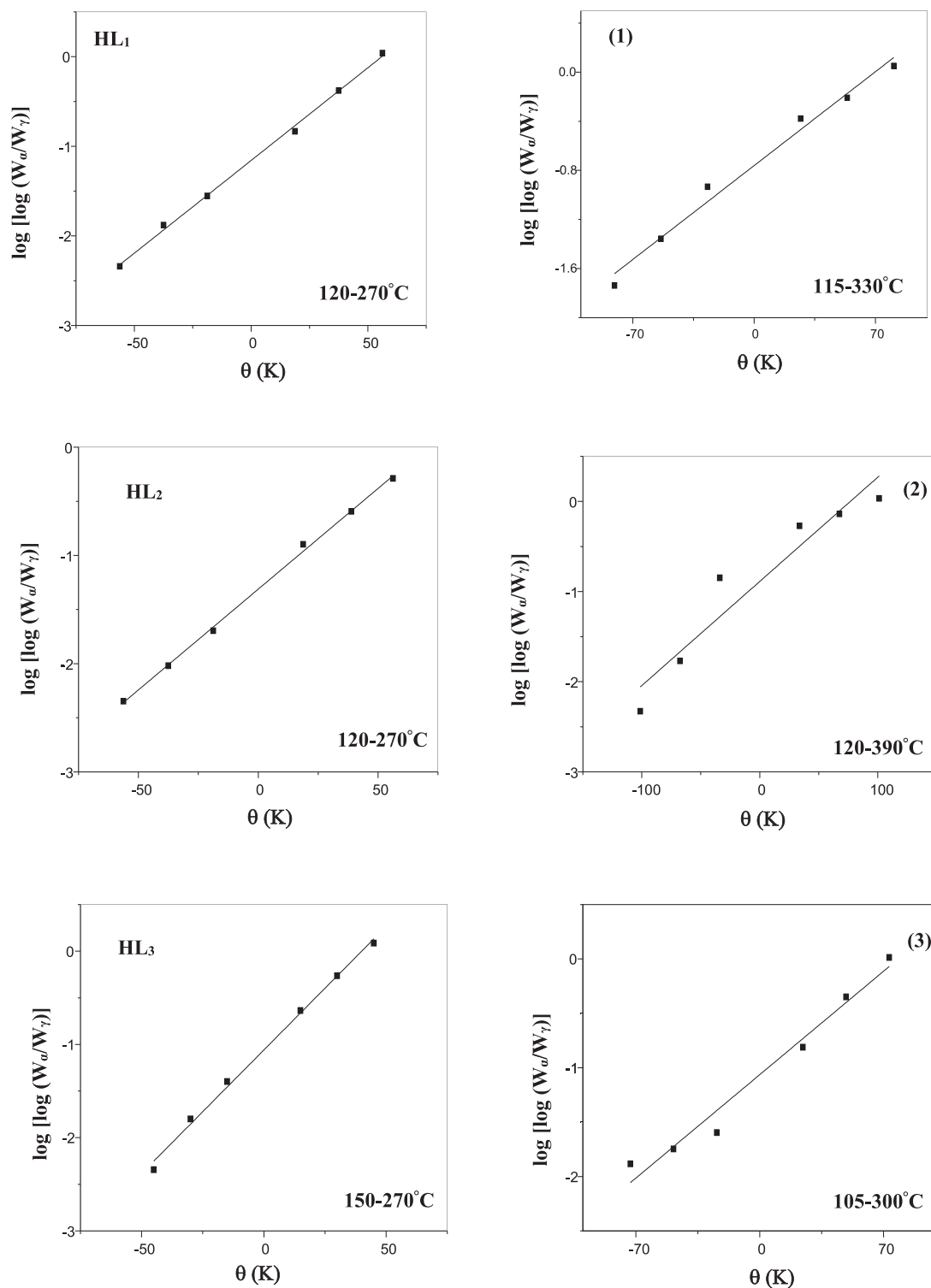


Fig. 7. Horowitz-Metzger (HM) of the ligands (HL_n) and their Cu(II) complexes (**1–3**).

binding) or to the major and minor grooves of DNA. Moreover, this “hyperchromic effect” can be explained on the basis of two phenomena. Firstly, the large surface area of the ligand as well as presence of planar aromatic chromophore facilitates a strong binding interaction of the ligands with CT-DNA thereby, providing ample opportunity for the complex to bind with the CT-DNA via, partial insertion of the aromatic moiety in between the stacking base pair. This groove binding results in structural reorganization of CT-DNA which entails partial unwinding

or damage of the double helix at the exterior phosphate backbone leading to the formation of a cavity to accommodate the complex [47]. The intrinsic binding constants (K_b) of all the ligands (HL_n) and Cu(II) complexes (**1–3**) with CT-DNA were determined (Eq. (1)) [48].

The K_b values obtained from the absorption spectral technique for ligands (HL_1 , HL_2 , and HL_3) were calculated as 5.86×10^5 , 3.05×10^5 and $1.63 \times 10^5 \text{ M}^{-1}$, respectively. The K_b values obtained from the absorption spectral technique for Cu(II) complexes (**1**, **2** and **3**)

Table 8
Kinetic parameters of the ligands (**HL_n**) and their Cu(II) complexes (**1–3**).

Compound ^a	Temp. (°C)	Method	Parameters					R
			E _a (kJ·mol ⁻¹)	A (s ⁻¹)	−ΔS* (J·mol ⁻¹ ·K ⁻¹)	ΔH* (kJ·mol ⁻¹)	ΔG* (kJ·mol ⁻¹)	
HL₁	120–270	CR	77.7	9.251 × 10 ⁵	1.34 × 10 ²	73.8	137	0.98907
		HM	86.8	5.741 × 10 ⁷	1.00 × 10 ²	82.9	130	0.99749
HL₂	120–270	CR	69.0	10 ⁴ × 6.12	1.57 × 10 ²	65.1	139	0.99291
		HM	78.1	5.54 × 10 ⁶	1.20 × 10 ²	74.2	130	0.99773
HL₃	150–270	CR	110	2.30 × 10 ⁹	6.97 × 10 ¹	106	139	0.99875
		HM	118	9.64 × 10 ¹⁰	3.86 × 10 ¹	114	133	0.99504
(1)	115–330	CR	42.4	7.04 × 10	2.14 × 10 ²	38.2	144	0.99389
		HM	51.4	1.63 × 10 ³	1.88 × 10 ²	47.2	140	0.98071
(2)	120–390	CR	52.4	3.29 × 10 ²	2.01 × 10 ²	48	154	0.92798
		HM	61.7	8.40 × 10 ³	1.75 × 10 ²	57	149	0.89703
(3)	105–300	CR	48.9	3.57 × 10 ²	2.00 × 10 ²	44.9	140	0.90914
		HM	58.8	2.26 × 10 ⁴	1.65 × 10 ²	54.9	134	0.96543

^a Numbers as given in Table 1.

were calculated as 6.84×10^5 , 4.51×10^5 and $3.67 \times 10^5 \text{ M}^{-1}$, respectively (Figs. 8 and 9). The binding constant of the complexes (**1–3**) are comparatively lower than that of the ligands (**HL_n**), may be due

to the ligands considering that the phenolic —OH group may enhance their affinity towards DNA binding through formation of hydrogen bonding [33].

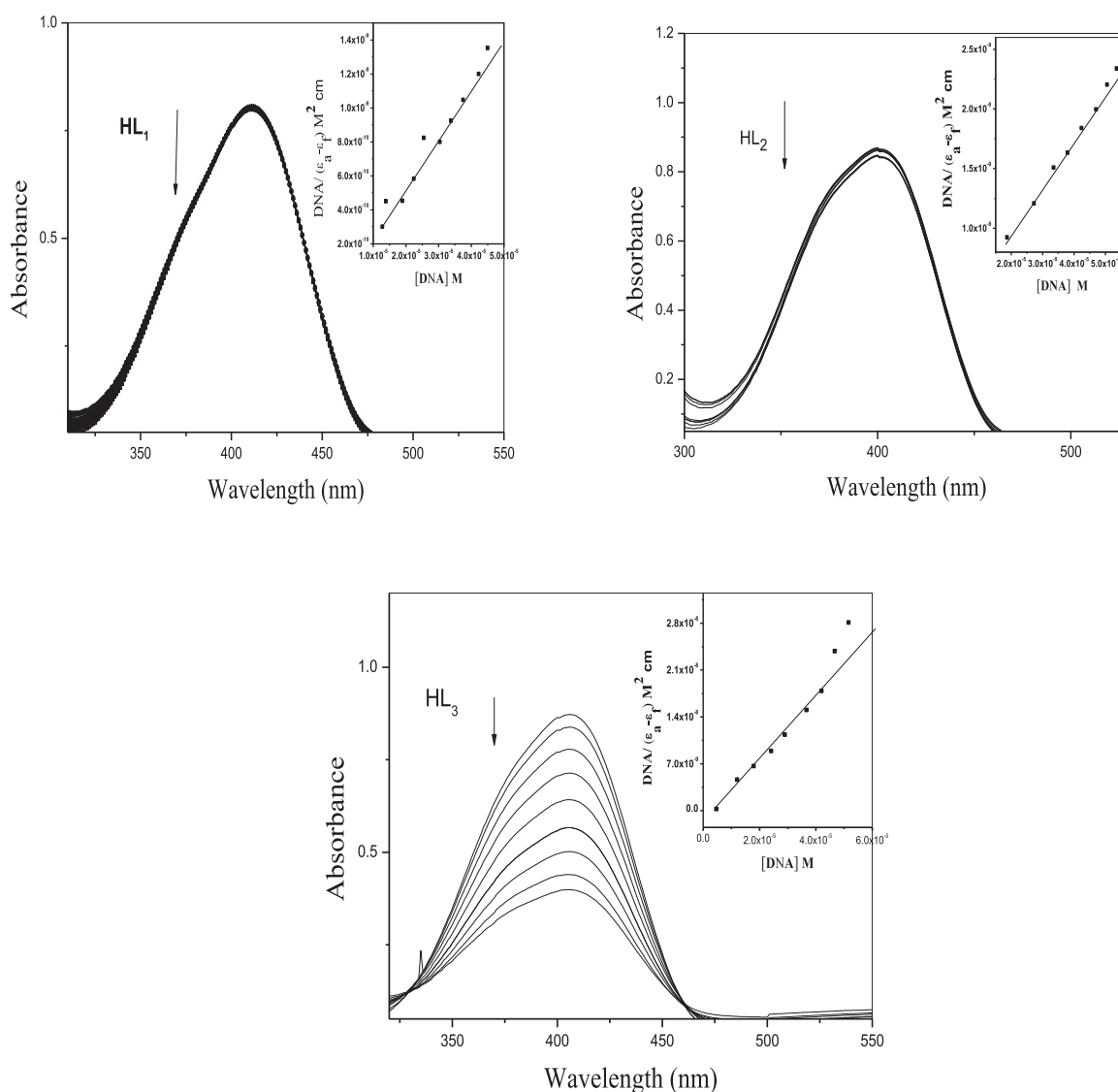


Fig. 8. Absorption spectra of ligands (**HL₁–HL₃**) in buffer pH 7.2 at 25 °C in the presence of increasing amount of CT-DNA. Arrows indicate the changes in absorbance upon increasing the CT-DNA concentration. Inset: plot of $[\text{DNA}]/(\epsilon_a - \epsilon_f) \times 10^{-8} \text{ M}^2 \cdot \text{cm}$ vs. $[\text{DNA}] \times 10^{-5} \text{ M}$ for titration of DNA with ligands (**HL_n**).

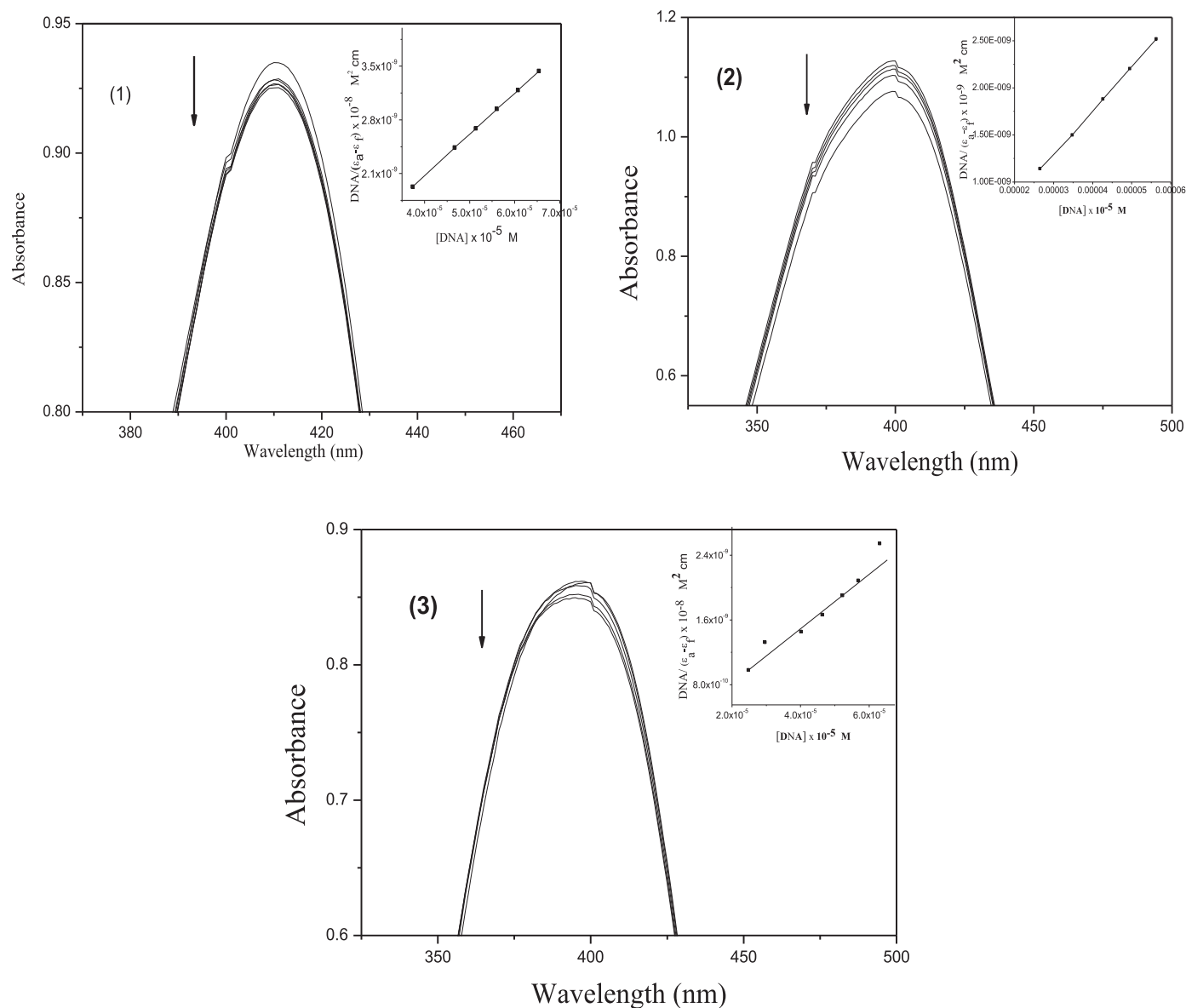


Fig. 9. Absorption spectra of complexes (1–3) in buffer pH 7.2 at 25 °C in the presence of increasing amount of CT-DNA. Arrows indicate the changes in absorbance upon increasing the CT-DNA concentration. Inset: plot of $[DNA] / (\epsilon_a - \epsilon_t) \times 10^{-8} \text{ M}^2 \text{ cm}$ vs. $[DNA] \times 10^{-5} \text{ M}$ for titration of CT-DNA with complexes (1–3).

3.8.2. Viscosity measurements

In addition to spectroscopic data, viscosity experiment was carried out which is regarded as less ambiguous and the most critical tests of DNA binding model in solution. A significant increase in the viscosity of DNA on the addition of a complex indicates the classical intercalative mode of binding to DNA. The binding of Cu(II) complexes with CT-DNA was further elucidated by measuring the relative specific viscosity of DNA after the addition of varying concentration of complexes. To further investigate the interaction mode of the binding mode of Cu(II) complexes (1–3) with DNA, a viscosity study was carried out at 25 °C. Viscosity experimental results clearly showed that the relative viscosity of CT-DNA increases steadily on addition of increasing concentration of Cu(II) complexes (1–3). The increased degree of viscosity, which may depend on its affinity to DNA follows the order of $3 > 2 > 1$ (Fig. 10). This observation can be explained on the fact that, classical intercalation model demands that the DNA helix must lengthen as base pairs are separated to accommodate the binding complexes, leading to the increase of DNA viscosity, as for the behaviors of the known DNA intercalators [33]. The result

further suggests an intercalating binding mode of the complexes with DNA and also parallels the above spectroscopic results, such as hypochromism and red shift of the complexes in the presence of DNA.

3.9. Antimicrobial activity

The antimicrobial activity of ligands (HL_n) and Cu(II) complexes (1–3) were tested against bacteria and fungi for detecting their antimicrobial activities [49–50]. The used organisms in the present investigation included *Escherichia coli* bacteria, Gram positive *Staphylococcus aureus* and *Candida albicans*. The results of the antibacterial activities of the synthesized compounds are recorded in Table 9. All ligands and complexes were found to have antibacterial activity against *Escherichia coli* except complex (1) (inhibition zone = 8 mm with activity index 32.0% for HL_2 , inhibition zone = 13 mm with activity index 52.0% for HL_1 , inhibition zone = 6 mm with activity index 24.0% for HL_3 , inhibition zone = 9 mm with activity index 36.0% for complex (2), inhibition

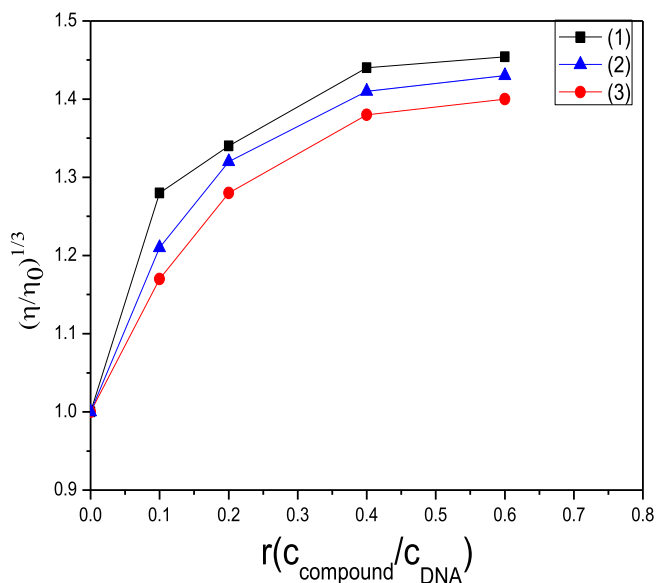


Fig. 10. Effect of increasing amounts of Cu(II) complexes (1–3) on the relative viscosity of DNA at 30 °C.

zone = 3 mm with activity index 12.0% for complex (1) and no activity for complex (3).

All the compounds under investigation have antibacterial activity against *Staphylococcus aureus* (inhibition zone = 11 mm with activity index 47.8% for **HL₂**, inhibition zone = 18 mm with activity index 78.3% for **HL₁**, inhibition zone = 5 mm with activity index 21.7% for **HL₃**, inhibition zone = 16 mm with activity index 69.6% for complex (2), inhibition zone = 8 mm with activity index 34.8% for complex (1) and inhibition zone = 2 mm with activity index 8.7% for complex (3).

All the compounds under investigation have antifungal activity against *Candida albicans* (inhibition zone = 16 mm with activity index 61.5% for **HL₂**, inhibition zone = 21 mm with activity index 80.8% for **HL₁**, inhibition zone = 8 mm with activity index 30.8% for **HL₃**, inhibition zone = 19 mm with activity index 73.1% for complex (1), inhibition zone = 14 mm with activity index 53.8% for complex (2) and inhibition zone = 10 mm with activity index 38.5% for complex (3). Ligand (**HL₁**) is the highest antibacterial activity against *Escherichia coli* as shown in Fig. 11.

3.10. Cytotoxic activity

The synthesized ligands and complexes have been evaluated for in vitro cytotoxic activity against two human cancer cell lines; HePG-2 (hepatocellular carcinoma) and MCF-7 (breast cancer). Inhibitory activity against HePG-2 and MCF-7 cell lines was detected by using different concentrations (i.e., 100, 50, 25, 12.5, 6.25, 3.125, 1.56 and 0 µg) of the

Table 9
Antibacterial and antifungal activities data of ligands (**HL_n**) and Cu(II) complexes (1–3).

Compound	<i>E. coli</i>		<i>S. aureus</i>		<i>C. albicans</i>	
	Diameter of inhibition zone (mm)	% Activity index	Diameter of inhibition zone (mm)	% Activity index	Diameter of inhibition zone (mm)	% Activity index
HL₁	13	52.0	18	78.3	21	80.8
HL₂	8	32.0	11	47.8	16	61.5
HL₃	6	24.0	5	21.7	8	30.8
(1)	3	12.0	8	34.8	14	53.8
(2)	9	36.0	16	69.6	19	73.1
(3)	NA	–	2	8.7	10	38.5
Ampicillin	25	100	23	100	NA	–
Clotrimazole	NA	–	NA	–	26	100

“NA”: no activity.

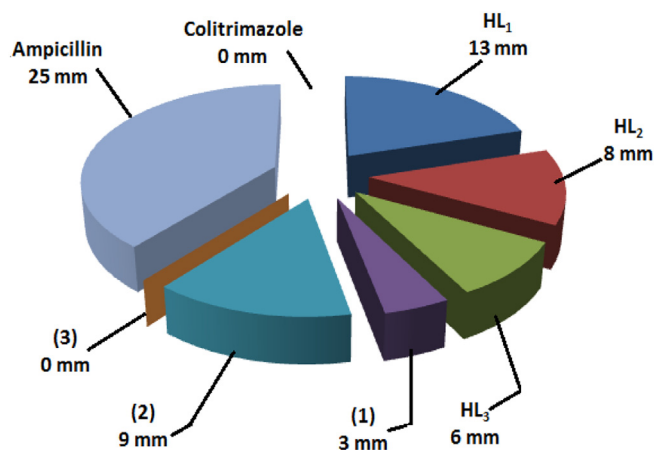


Fig. 11. Antibacterial activity data of ligands (**HL_n**) and Cu(II) complexes (1–3) against *Escherichia coli*.

Table 10

Inhibition of cell viability of Ligands and complexes against HePG-2 and MCF-7 cells in comparison with standard Doxorubicin (DOX).

Compound	Cell lines [IC ₅₀ (µg/mL)]	
	HePG-2	MCF-7
DOX	4.50 ± 0.3	4.17 ± 0.2
HL₁	6.88 ± 0.5	7.60 ± 0.9
HL₂	27.19 ± 2.3	14.65 ± 1.5
HL₃	58.10 ± 3.4	63.13 ± 3.6
(1)	41.77 ± 2.7	26.57 ± 1.9
(2)	11.80 ± 1.3	9.38 ± 1.0
(3)	67.66 ± 3.8	46.75 ± 3.1

Data presented as mean ± SD. IC₅₀ (µg/mL): 1–10 (very strong), 11–20 (strong), 21–50 (moderate), 51–100 (weak) and above 100 (non-cytotoxic).

Table 11

Results of radical scavenging activity and % of inhibition of each ligands (**HL_n**) and Cu(II) complexes (1–3) by ABTS method.

No.	Method	ABTS Abs(control) – Abs(test) / Abs(control) × 100
Compounds	Absorbance of samples	% inhibition
Control of ABTS	0.510	0%
Ascorbic-acid	0.058	88.6%
HL₁	0.353	30.8%
HL₂	0.367	28.0%
HL₃	0.382	25.1%
(1)	0.369	27.6%
(2)	0.358	29.8%
(3)	0.374	26.7%

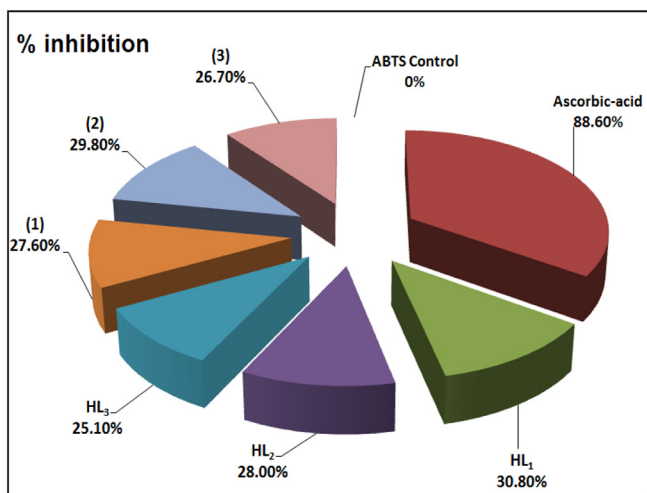


Fig. 12. The inhibition percentage of ligands (HL_n) and Cu(II) complexes (1–3) and standard ascorbic acid.

tested compounds and viability cells (%) were determined by the colorimetric method. Also, inhibitory concentration 50 (IC_{50}) was calculated and presented in Table 10. The results clearly revealed that HL_1 possessed very good cytotoxic activity against the hepatocellular carcinoma (HePG-2) and mammary gland breast cancer (MCF-7) cell lines ($IC_{50} = 6.88 \pm 0.5$ and $7.60 \pm 0.9 \mu\text{g/mL}$, respectively). HL_2 exhibiting good cytotoxic activity against the hepatocellular carcinoma (HePG-2) and mammary gland breast cancer (MCF-7) cell lines ($IC_{50} = 27.19 \pm 2.3$ and $14.65 \pm 1.5 \mu\text{g/mL}$, respectively). HL_3 exhibiting weak cytotoxic activity against both the hepatocellular carcinoma (HePG-2) and mammary gland breast cancer (MCF-7) cell lines. Also Cu(II) complex (2) possessed very good cytotoxic activity against the hepatocellular carcinoma (HePG-2) and mammary gland breast cancer (MCF-7) cell lines

($IC_{50} = 18.8 \pm 1.3$ and $9.38 \pm 1.0 \mu\text{g/mL}$, respectively). Cu(II) complex (1) exhibiting good cytotoxic activity against the hepatocellular carcinoma (HePG-2) and mammary gland breast cancer (MCF-7) cell lines ($IC_{50} = 41.77 \pm 2.7$ and $26.57 \pm 1.9 \mu\text{g/mL}$, respectively). Cu(II) complex (3) exhibiting weak cytotoxic activity against both the hepatocellular carcinoma (HePG-2) and mammary gland breast cancer (MCF-7) cell lines. Comparing results with standard Doxorubicin (DOX) response indicated HL_1 have highest cytotoxic activity than HL_2 and HL_3 , also Cu(II) complexes (2) have highest cytotoxic activity than Cu(II) complexes (1) and (3).

3.11. Antioxidant activity

Antioxidants are chemical substances that donate an electron to the free radical and convert it to a harmless molecule. They may reduce the energy of the free radical or suppress radical formation or break chain propagation or repair damage and reconstitute membranes [51,52].

Table 11 expressed results of radical scavenging ability and percentage of inhibition of each ligands (HL_n), their Cu(II) complexes (1–3) and standard ascorbic acid, as a reference compound by ABTS method as shown in Fig. 12. The results showed that all the ligands have good antioxidant activity (% inhibition value = 30.8, 28.0 and 25.1% for HL_1 , HL_2 and HL_3 , respectively). The antioxidant activity of Cu(II) complexes are (% inhibition value = 27.6, 29.8 and 26.7% for the (1), (2) and (3) complexes, respectively).

3.12. Molecular docking study

Molecular docking is a key tool in computer drug design [53]. The focus of molecular docking is to simulate the molecular recognition process. Molecular docking aims to achieve an optimized conformation for both the protein and drug with relative orientation between them such that the free energy of the overall system is minimized. In this work, we used molecular docking between ligands (HL_n) and prostate cancer (3qum). The results showed a possible arrangement between ligands

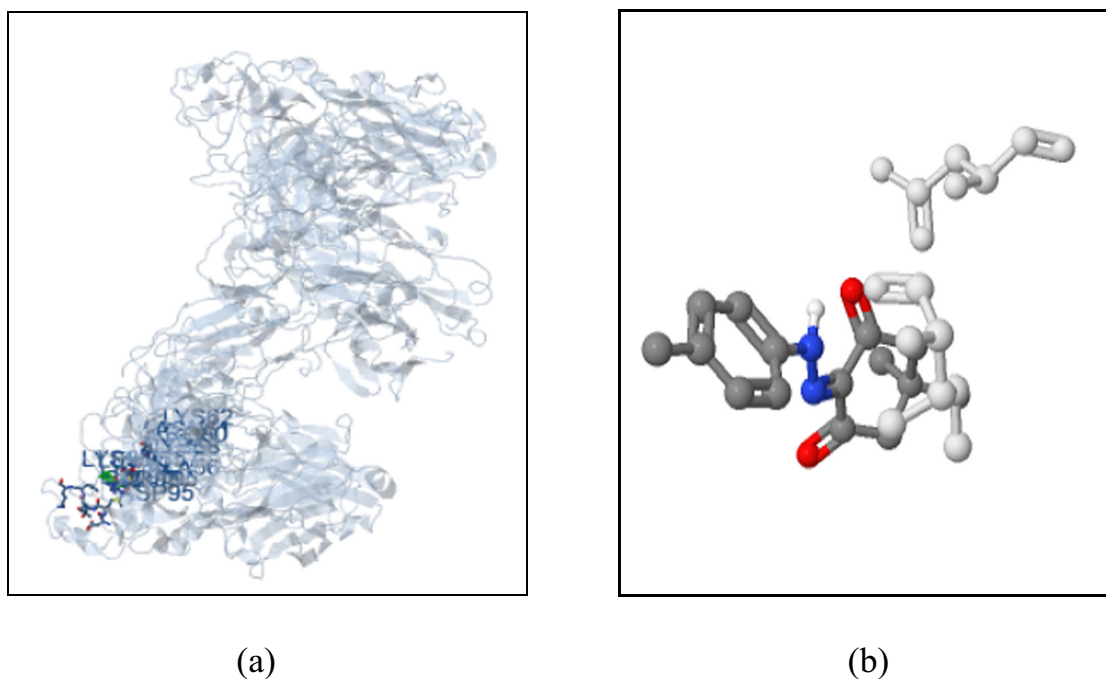


Fig. 13. The ligand (HL_1) (green in (a) and blue in (b)) in interaction with receptor prostate cancer 3qum. (For interpretation of the references to color in this figure legend, the reader is referred to the web version of this article.)

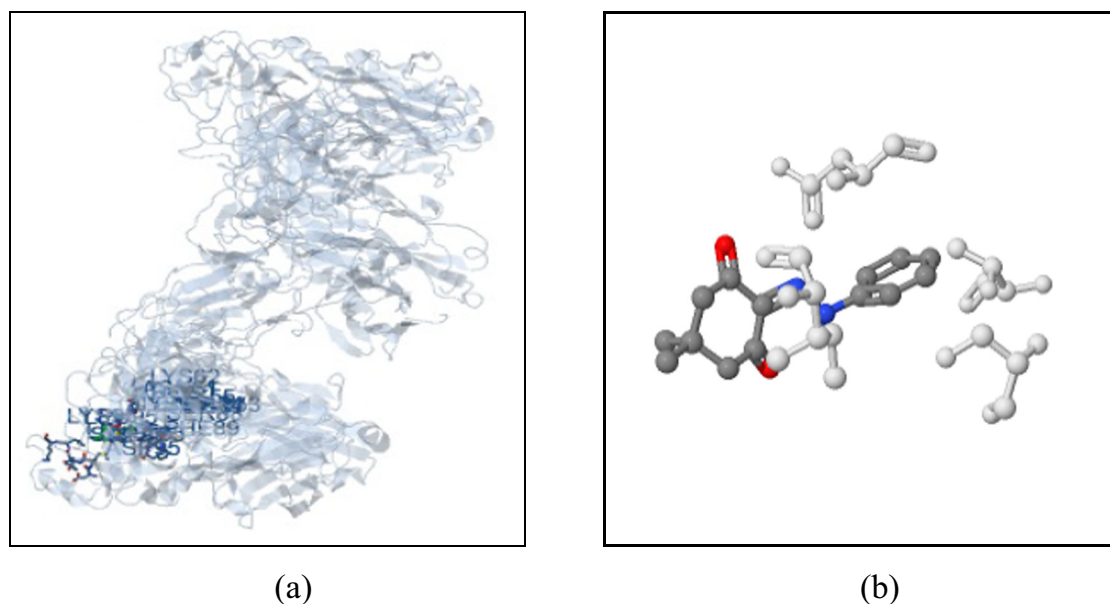


Fig. 14. The ligand (**HL₂**) (green in (a) and blue in (b)) in interaction with receptor prostate cancer 3qum. (For interpretation of the references to color in this figure legend, the reader is referred to the web version of this article.) (For interpretation of the references to color in this figure legend, the reader is referred to the web version of this article.)

and receptor 3qum. The docking study showed a favorable interaction between ligands and the receptor 3qum as shown in Figs. 13–15 and the calculated energy is listed in Table 12.

According to the results obtained in this study, HB plot curve indicate that the ligands (**HL_n**) bind to the protein with hydrogen bond interactions and decomposed interaction energies in kcal/mol were exist

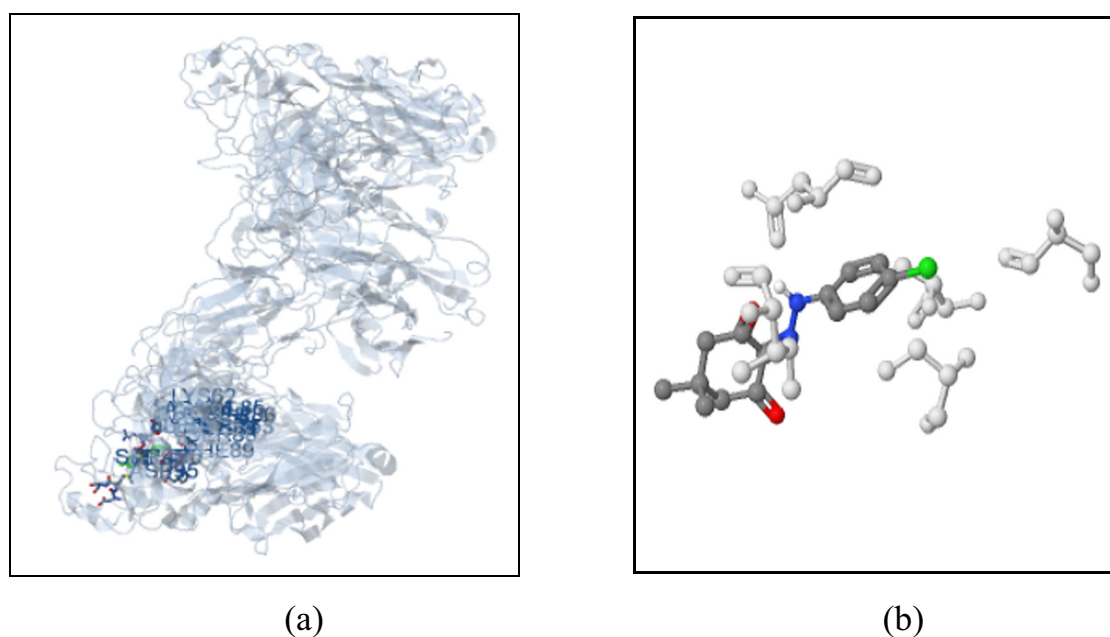


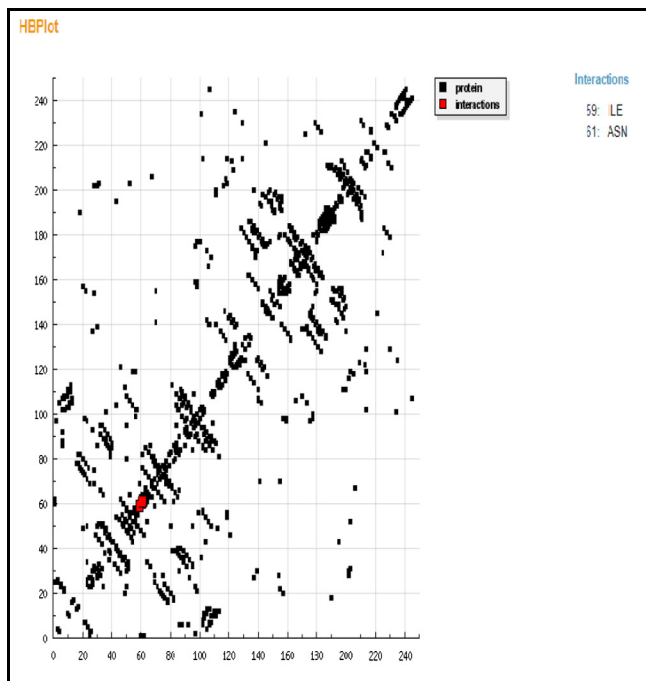
Fig. 15. The ligand (**HL₃**) (green in (a) and blue in (b)) in interaction with receptor prostate cancer 3qum. (For interpretation of the references to color in this figure legend, the reader is referred to the web version of this article.) (For interpretation of the references to color in this figure legend, the reader is referred to the web version of this article.)

Table 12
Energy values obtained in docking calculations of ligands (**HL_n**) with receptor prostate cancer 3qum.

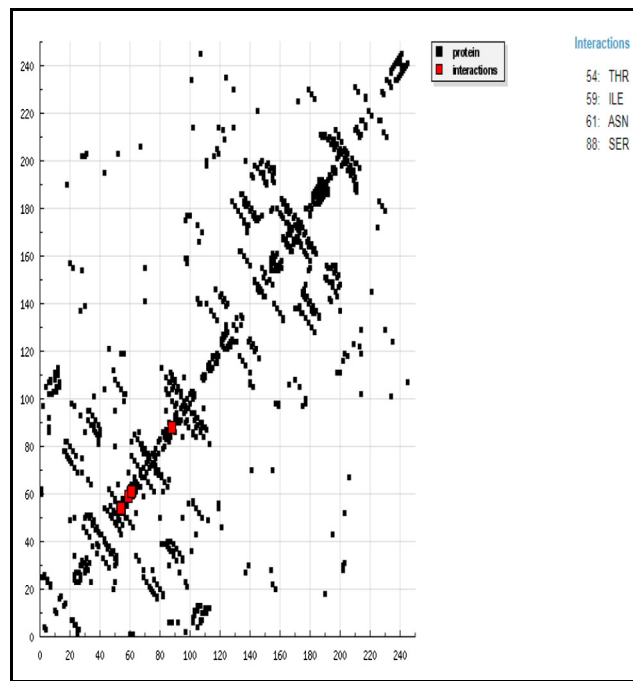
Compound	Gibbs. free energy of binding (kcal/mol)	Inhibition constant (K _i) (uM)	vdW + H bond + desolv energy (kcal/mol)	Electrostatic energy (kcal/mol)	Total intermolecular energy (kcal/mol)	Interact surface
(HL ₁)	−5.01	211.86	−5.19	−0.01	−5.19	540.04
(HL ₂)	−5.22	150.10	−5.36	−0.04	−5.40	572.406
(HL ₃)	−5.50	92.85	−5.84	−0.01	−5.85	531.801

between ligands with 3qum receptor as shown in Fig. 16. The calculated efficiency is favorable where K_i values estimated by AutoDock were compared with experimental K_i values, when available, and the Gibbs free energy is negative. Also, based on this data, we can propose that interaction between the 3qum receptor and the ligands is possible. 2D plot curves of docking with ligands are shown in Fig. 17(a–c). This interaction could activate apoptosis in cancer cells energy of interactions

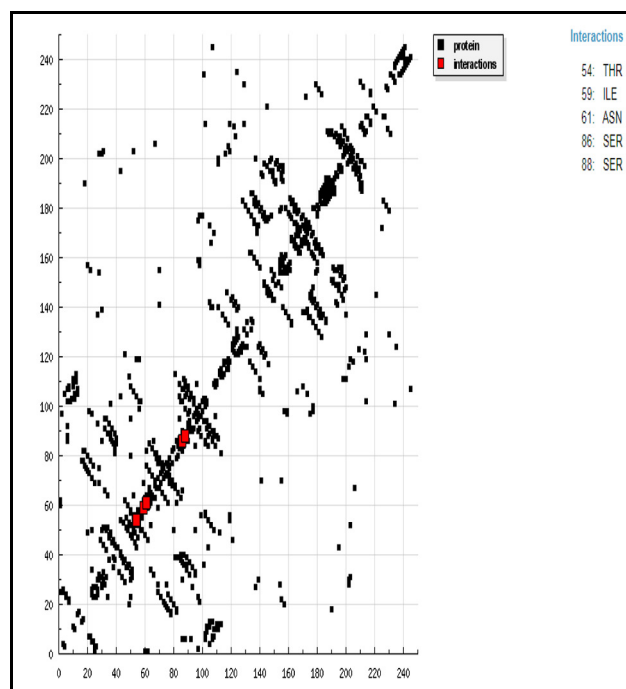
with ligands. Binding energies are most widely used as mode of measuring binding affinity of compounds. Thus, decrease in binding energy due to mutation will increase the binding affinity of the compounds towards the receptor. The characteristic features of compounds were represented in presence of active sites available for hydrogen bonding [54]. This feature gives them the ability to be good binding inhibitors to the protein and will help to produce augmented inhibitory compounds.



(a)

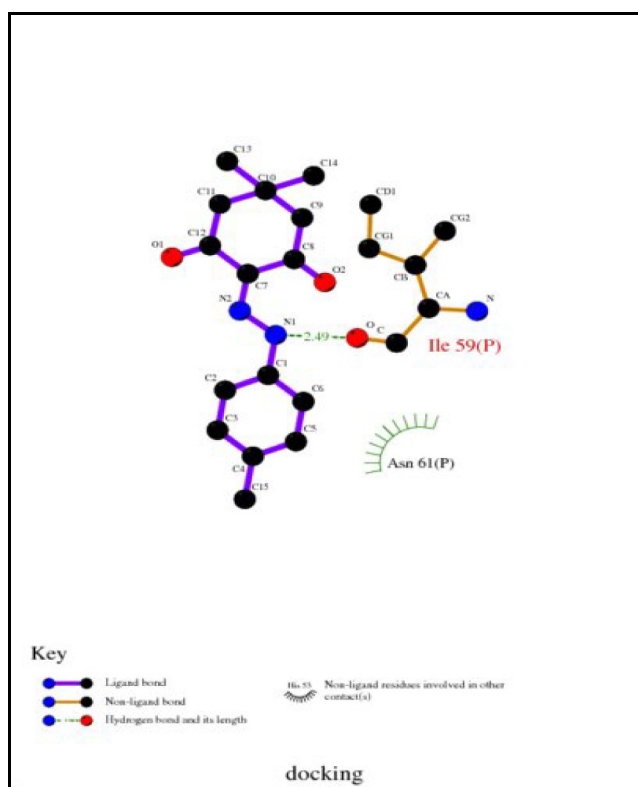


(b)

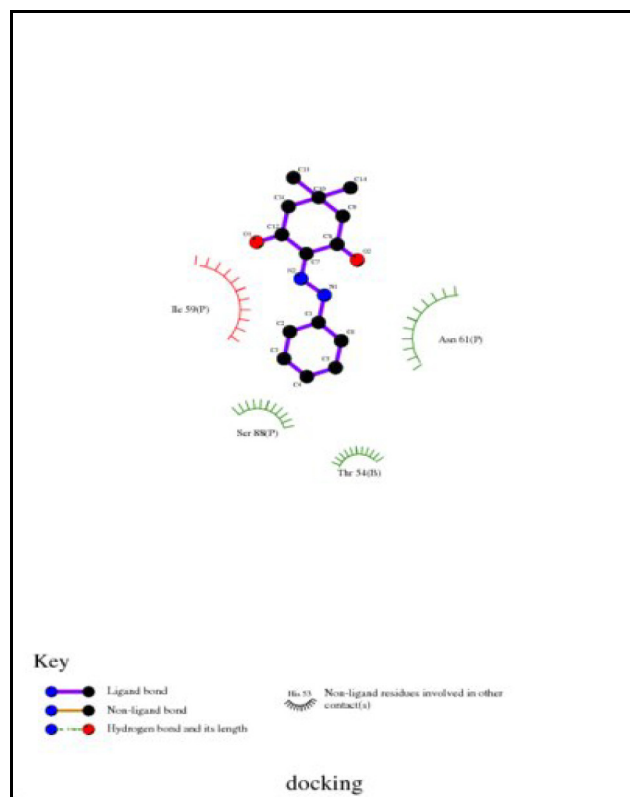


(c)

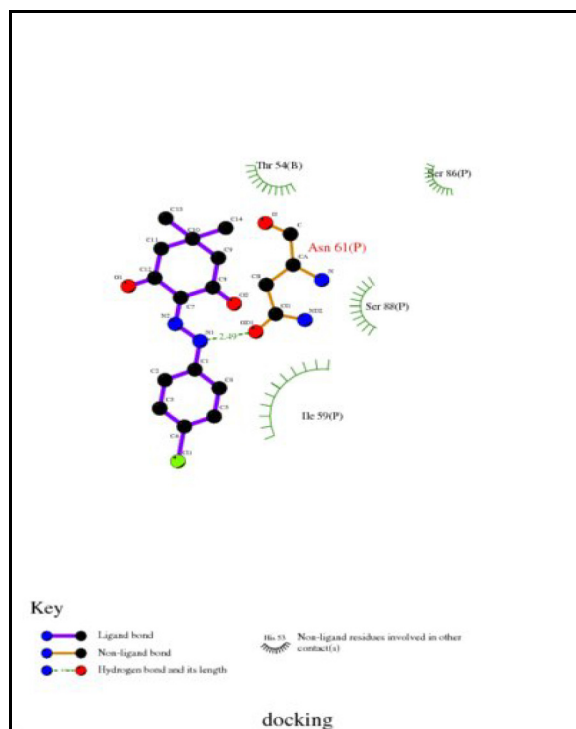
Fig. 16. HB plot of interaction between ligands (a) HL₁, (b) HL₂ and (c) HL₃ with receptor prostate cancer 3qum.



(a)



(b)



(c)

Fig. 17. 2D plot of interaction between ligands (a) HL₁, (b) HL₂ and (c) HL₃ with receptor prostate cancer 3qum.

The ligands **HL**₁, **HL**₂ and **HL**₃ showed binding energy -5.01 , -5.22 and -5.50 kcal/mol, respectively, with 3qum receptor prostate cancer using H-bond, electrostatic and Van der Waals interactions. On the basis of complex scoring and interactions with the active site residue and binding ability, it was deciphered that ligands (**HL**_n) could be promising inhibitors of 3qum - IMMUNE SYSTEM prostate cancer. This gives us the conclusion that **HL**₃ possess lowest binding energy (-5.50 kcal/mol) and highest binding ability.

4. Conclusion

This paper reports the synthesis, characterization, DNA binding and biological activity of the ligands and their Cu(II) complexes. Based on the spectroscopic, magnetic, thermal and theoretical data; the Cu(II) complexes (**1–3**) have square planar geometry in which the ligands behave as a monobasic bidentate and exist in an internally hydrogen bonded keto-hydrazone form rather than the azo-enol form. The energies of the HOMO and LUMO orbitals of Cu(II) complexes were negative which indicates that the complexes are stable. The thermogravimetric analysis of the compounds shows that the values of activation energies of decomposition (E_a) are found to be 76.8, 102 and 110 kJ/mol for the ligands **HL**₁, **HL**₂ and **HL**₃, respectively, and the values of E_a are found to be 30.5, 60.1 and 51.1 kJ/mol for the complexes **1**, **2** and **3**, respectively. The calf thymus DNA binding activity of the ligands (**HL**_n) and their Cu(II) complexes were studied by absorption spectra and viscosity measurements. Molecular docking was used to predict the binding between the compounds (**HL**_n) with 3qum-IMMUNE SYSTEM receptor of human prostate specific antigen (PSA) in a Fab sandwich with a high affinity and a PCa selective antibody. The antimicrobial activities of ligands were tested against Gram negative bacteria (*Escherichia coli*), Gram positive bacteria (*Staphylococcus aureus*) and fungal (*Candida albicans*).

References

- [1] E.V. Shchegol'kov, Y.V. Burgart, O.G. Khudina, V.I. Saloutin, O.N. Chupakhin, Russ. Chem. Rev. 79 (2010) 31–61.
- [2] T.V. Deepthi, P. Venugopalan, Inorg. Chim. Acta 450 (2016) 243–250.
- [3] G.D. Diana, P.M. Carabateas, R.E. Johnson, G.L. Williams, F. Pancic, J.C. Collins, J. Med. Chem. 21 (1978) 889–894.
- [4] J. Emsley, Struct. Bond. 57 (1984) 147–191.
- [5] W. Urbaniak, K. Jurek, K. Witt, A. Gorczko, B. Staniszewski, Chem. Aust. 65 (2011) 273–282.
- [6] M.M. Conradie, A.J. Muller, J. Conradie, S. Afr. J. Chem. 61 (2008) 13–21.
- [7] R.M. Mohareb, F.Q. Al Farouk, W.W. Wardakhan, Med. Chem. Res. 27 (2018) 1984–2003.
- [8] K.T. Mahmudov, R.A. Rahimov, M.B. Babanly, P.Q. Hasanov, F.G. Pashaev, A.G. Gasanov, M.N. Kopylovich, A.J.L. Pombeiro, J. Mol. Liq. 162 (2011) 84–88.
- [9] G. Gilli, P. Gilli, The Nature of the Hydrogen Bond. Outline of a Comprehensive Hydrogen Bond Theory, Oxford University Press, 2009.
- [10] K.T. Mahmudov, M.N. Kopylovich, A.J.L. Pombeiro, Coord. Chem. Rev. 257 (2013) 1244–1281.
- [11] M.N. Kopylovich, T.C.O. Mac Leod, K.T. Mahmudov, M.F.C. Guedes da Silva, A.J.L. Pombeiro, Dalton Trans. 40 (2011) 5352–5361.
- [12] J.D.C. Almeida, D.A. Paixão, I.M. Marzano, J. Ellena, M. Pivatto, N.P. Lopes, A.M.D.C. Ferreira, E.C. Pereira-Maia, S. Guillard, W. Guerra, Polyhedron 89 (2015) 1–8.
- [13] K. Azizi, N. Esfandiary, M. Karimi, M. Kazemi, A. Heydari, Appl. Organomet. Chem. 31 (2017), e3658.
- [14] G.A. Bhat, R. Maqbool, A.A. Dar, M. Ul Hussain, R. Murugavel, Dalton Trans. 46 (2017) 13409–13420.
- [15] R. Shirley, The CRYSPFIRE System for Automatic Powder Indexing: User's Manual, The Lattice Press, 41 Guildford Park Avenue, Guildford, Surrey GU2 7NL, England, 2000.
- [16] M.S. Jambí, J. Mol. Struct. 1143 (2017) 217–228.
- [17] H.C. Yao, J. Org. Chem. 29 (1964) 2959–2963.
- [18] K.T. Mahmudov, M.N. Kopylovich, M.F. da Silva, G.S. Mahmudova, M. Sutradhar, A.J.L. Pombeiro, Polyhedron 60 (2013) 78–84.
- [19] M.N. Kopylovich, K.T. Mahmudov, M. Haukka, K.V. Luzyanin, A.J.L. Pombeiro, Inorg. Chim. Acta 374 (2011) 175–180.
- [20] D.-D. Li, N. Zhang, Z. Yang, Z.-W. Tao, Appl. Organomet. Chem. 31 (2017), e3548.
- [21] M.F. Reichmann, S.A. Rice, C.A. Thomas, P. Doty, J. Am. Chem. Soc. 76 (1954) 3047–3053.
- [22] A. Wolfe, G.H. Shimer, T. Meehan, Biochemistry 26 (1987) 6392–6396.
- [23] S. Satyanaryana, J.C. Dabrowial, J.B. Chaires, Biochemistry 32 (1993) 2573–2584.
- [24] N.M.R. Martins, S. Anbu, K.T. Mahmudov, R. Ravishankaran, M.F.C. Guedes Da Silva, L.M.D.R.S. Martins, A.A. Karande, A.J.L. Pombeiro, New J. Chem. 41 (2017) 4076–4086.
- [25] Y. Xiong, X.F. He, X.H. Zou, J.Z. Wu, X.M. Chen, L.N. Ji, R.H. Li, Y.J. Zhou, R.B. Yu, J. Chem. Soc. Dalton Trans. 1 (1999) 19–24.
- [26] P.H. De Azambuja Carvalho, A.R. Duval, F.R. Manzolli Leite, F. Nedel, W. Cunico, R.G. Lund, J. Enzyme Inhib. Med. Chem. 31 (2016) 126–131.
- [27] H.K. Gencer, U.A. Cevik, S. Levent, B.N. Saglik, B. Korkut, Y. Özkay, S. Ilgin, Y. Öztürk, Molecules 22 (2017), E507.
- [28] R. Konakanchi, R. Mallela, R. Guda, L.R. Kotha, Res. Chem. Intermed. 7 (2017) 1–27.
- [29] G.A. Gamov, M.N. Zavalishin, V.A. Sharnin, Spectrochim. Acta A 206 (9) (2019) 160–164.
- [30] A.F. Shoair, A.A. El-Bindary, M.K. Abd El-Kader, J. Mol. Struct. 1143 (2017) 100–115.
- [31] K.T. Mahmudov, M. Sutradhar, L.M.D. Martins, M.F.C. da Silva, A. Ribera, A.V.M. Nunes, S.I. Gahramanova, F. Marchetti, A.J.L. Pombeiro, RSC Adv. 5 (2015) 25979–25987.
- [32] M.K. Renuka, V. Gayathri, Catal. Commun. 104 (2018) 71–77.
- [33] I.M. El-Deen, A.F. Shoair, M.A. El-Bindary, J. Mol. Liq. 249 (2017) 533–545.
- [34] M. Azarkish, A. Akbari, T. Sedaghat, J. Simpson, J. Mol. Struct. 1156 (2018) 34–42.
- [35] M. del Mar Conejo, J. Cantero, A. Pastor, E. Álvarez, A. Galindo, Inorg. Chim. Acta 470 (2018) 113–118.
- [36] A. Akinci, D.B. Celepci, L. Karadeniz, N. Korkmaz, M. Aygün, S.T. Astley, Appl. Organomet. Chem. 31 (2017), e3831.
- [37] N. Nakamoto, Infrared Spectra and Raman Spectra of Inorganic and Coordination Compounds, 5th ed. Wiley, New York, 1997.
- [38] A.B.P. Lever, Inorganic Electronic Spectroscopy, 2nd ed. Elsevier, Amsterdam, 1984.
- [39] M.N. Kopylovich, K.T. Mahmudov, M.F.C. Guedes da Silva, P.J. Figiel, Y.Y. Karabach, M.L. Kuznestov, K.V. Luzyanin, A.J.L. Pombeiro, Inorg. Chem. 50 (2011) 918–931.
- [40] C. Hammond, The Basics of Crystallography and Diffraction, 3rd ed. Oxford University Press, 2009.
- [41] N.A. El-Ghamaz, A.A. El-Bindary, R.A. El-Boz, Synth. Met. 226 (2017) 207–214.
- [42] M.K. Koley, O.P. Chouhan, S. Biswas, J. Fernandes, A. Banerjee, A. Chattopadhyay, B. Varghese, P.T. Manoharan, A.P. Koley, Inorg. Chim. Acta 456 (2017) 179–198.
- [43] A.W. Coats, J.P. Redfern, Nature 20 (1964) 68–79.
- [44] H.W. Horowitz, G. Metzger, Anal. Chem. 35 (1963) 1464–1468.
- [45] A.A. El-Bindary, N. Hassan, M.A. El-Affify, J. Mol. Liq. 242 (2017) 213–228.
- [46] M. Mohanraj, G. Ayyannan, G. Raja, C. Jayabalakrishnan, Appl. Organomet. Chem. 31 (4) (2017), e3582.
- [47] M. Sakthi, A. Ramu, J. Mol. Struct. 1149 (2017) 727–735.
- [48] L.H. Abdel-Rahman, A.M. Abu-Dief, N.M. Ismail, M. Ismael, Inorg. Nano-Metal Chem. 47 (2017) 467–480.
- [49] M.I. Abou-Dobara, A.Z. El-Sonbati, Sh.M. Morgan, World J. Microbiol. Biotechnol. 29 (2013) 119–126.
- [50] N.H. Metwally, M.A. Abdalla, M.A.N. Mosselhi, E.A. El-Desoky, Carbohydr. Res. 345 (2010) 1135–1141.
- [51] Z.H. Chen, C.J. Zheng, L.P. Sun, H.R. Piao, Eur. J. Med. Chem. 45 (2010) 5739–5743.
- [52] R.S. Cotran, V. Kumar, T. Collins, Robbins's Pathological Basis of Diseases, 6th ed. Thomson Press (I) Ltd., Noida and India, 1999.
- [53] S.K. Mondal, G. Chakraborty, M. Gupta, U.K. Mazumdar, Indian J. Exp. Biol. 44 (2006) 39–44.
- [54] A. Beteringhe, C. Racuciu, C. Balan, E. Stoican, L. Patron, Adv. Mater. Res. 787 (2013) 236–240.